Angewandte Chemie
Eine Zeitschrift der Gesellschaft Deutscher Chemiker

Supporting Information

Lewis Acid Coordination Redirects S-Nitrosothiol Signaling Output

Valiallah Hosseininasab, Alison C. McQuilken, Abolghasem (Gus) Bakhoda, Jeffery A. Bertke, Qadir K. Timerghazin, and Timothy H. Warren**

anie_202001450_sm_miscellaneous_information.pdf

Supporting Information

Table of Contents

General Instrumentation and Physical Methods

All experiments were carried out under dry nitrogen atmosphere by utilizing MBraun gloveboxes and/or standard Schlenk techniques unless otherwise mentioned. ^{1}H and ^{19}F NMR and $^{13}C\{^{1}H\}$ NMR spectra were recorded on a Varian 400 MHz spectrometer at room temperature unless otherwise noted. Variable temperature ^{15}N NMR experiments were recorded on a Varian 400 MHz spectrometer at -70 °C to 20 °C range. The chemical shift (δ) values are expressed in ppm relative to tetramethylsilane, whereas the residual ^{1}H signal of deuterated solvent served as an internal standard. Elemental analyses were performed on a Perkin-Elmer PE2400 micro-analyzer at Georgetown University. UV-vis spectra were recorded on Agilent 8454 Diode Array spectrometer equipped with stirrer and Unisoku USP-203 cryostat. The molar extinction coefficients of different isolated complexes were determined from Beer's law plots (absorbance *vs* concentration) with at least four different concentrations. IR spectra (with spectral resolution of 2 cm^{-1}) were collected on an ATR spectrometer. Details for X-ray crystallography appear in Section 15.

2. Materials

All chemicals were purchased from common vendors (e.g. Sigma-Aldrich, Acros Organics, Strem Chemicals, TCI) and used without further purification unless otherwise mentioned. $MesCH_2SH$ and Tetrabutylammonium tetraphenylborate ($[NBu_4][BPh_4]$ were obtained from Sigma-Aldrich and tris(pentafluorophenyl)borane was obtained from Boulder Scientific Company and used without further purification. Molecular sieves (4A, 4-8 mesh beads) were obtained from Fisher Scientific and were activated prior to use in vacuo at 200 °C for 24 h. Extra dry solvents (≥99.5%) with Acroseal® and deuterated solvents were purchased from Acros Organics and Cambridge Isotope Laboratories, respectively. Both anhydrous and deuterated solvents were sparged with nitrogen and stored over activated 4A molecular sieves under a nitrogen atmosphere. Nitric oxide gas (unlabeled) was obtained from Praxair and purified by passing through a column of Ascarite (8-20 mesh) purchased from Sigma.

3. Synthesis and Characterization of AdSNO (1)

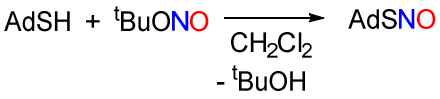

Scheme S1. Synthesis of AdSNO (**1**).

The synthesis of AdSNO has been previously reported,[1] but we include full characterization data here to allow for careful comparison between AdSNO and its tris(pentafluorophenyl)borane adduct AdSNO-B(C_6F_5)$_3$.

^{t}BuONO (1.225 g, 11.883 mmol) was directly added to a solution of AdSH (0.5 g, 2.97 mmol) in dichloromethane (*ca.* 3 mL). The solution was stirred for 0.5 h at RT and the resultant dark green solution was dried to obtain a dark green solid (0.530 g, 2.686 mmol) in 90% yield.

Ad^{15}NO was prepared analogously from ^{t}BuO^{15}NO.[2]

^{1}H NMR (400 MHz, 298 K, $CDCl_3$): δ 2.54 (d, 6H, CH_2), 2.29 (t, 3H, C*H*), 1.93 (d, 6H, CH_2) (Figure S1);

^{13}C{^{1}H} NMR (100 MHz, 298 K, $CDCl_3$): δ 55.77, 43.60, 36.38, 30.11.

^{15}N NMR (41 MHz, 20 °C, CD_2Cl_2): δ 839.60 (s, Ad^{15}NO) (Figure S2).

^{15}N NMR (41 MHz, -70 °C, CD_2Cl_2): δ 845.35 (s, *anti*, Ad^{15}NO), δ 786.56 (s, *syn*, Ad^{15}NO) (Figure S3).

UV-Vis (CH_2Cl_2, 25 °C): λ_{max}/nm (ε/M^{-1}cm^{-1}) = 561 (5), 601 (13) (Figure S4).

FT-IR (cm^{-1}): 1486 ν(^{14}NO); 645 ν(S-^{14}N); 1455 ν(^{15}NO); 629 ν(S-^{15}N); Hooke's law predicts $^{15N/14N}\Delta\nu$ = 27 cm^{-1} and $^{15N/14N}\Delta\nu$ = 15, respectively (Figure S5). The IR spectra were taken by putting AdSNO as a fine powder directly on the ATR instrument.

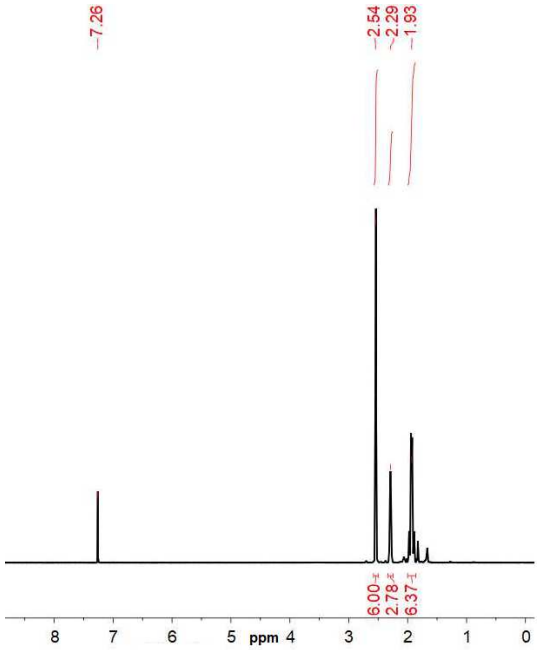

Figure S1. ^{1}H NMR spectrum (400 MHz, 25 °C, $CDCl_3$) of AdSNO (**1**).

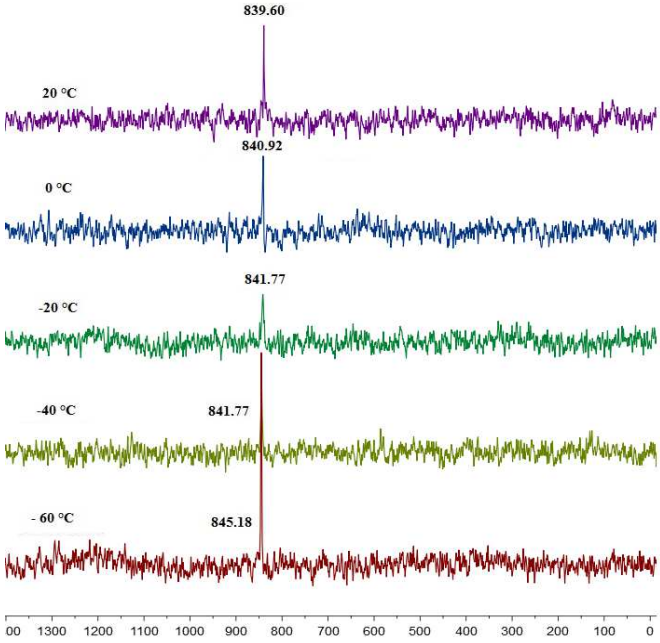

Figure S2. Variable temperature ^{15}N NMR spectra (41 MHz, CD_2Cl_2) of AdS^{15}NO (**1**-^{15}**N**).

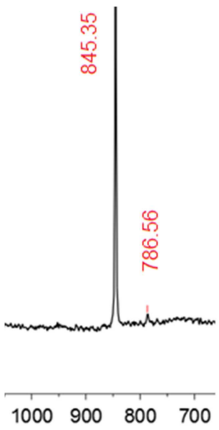

Figure S3. ^{15}N NMR spectrum (41 MHz, CD_2Cl_2) of AdS^{15}NO (**1**-^{15}**N**) at -70 °C.

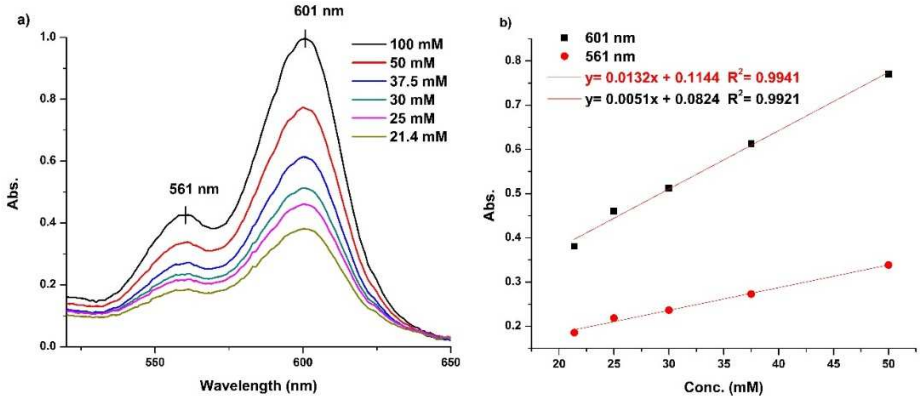

Figure S4. (a) UV-Vis spectra of AdSNO (**1**) in dichloromethane at 25 °C at different concentrations. (b) Beer's law plot for (**1**) depicts λ_{max} = 561 nm (ε = 5 $M^{-1}cm^{-1}$) and λ_{max} = 601 nm (ε = 13 $M^{-1}cm^{-1}$)

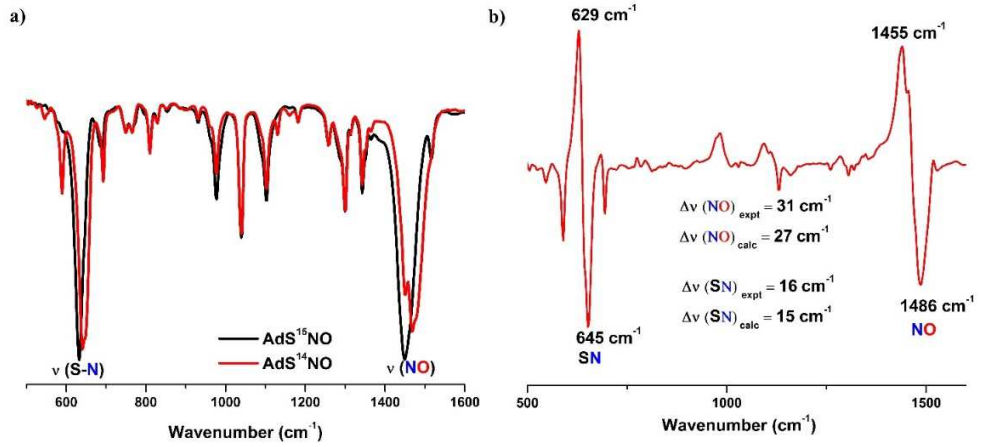

Figure S5. a) FT-IR spectra of AdS^{14}NO (**1**) (red trace) and AdS^{15}NO (**1**-^{15}**N**) (black trace). b) The difference spectrum between (**1**) (down) and (**1**-^{15}**N**) (up).

4. Synthesis and Characterization of $MesCH_2SNO$ (2)

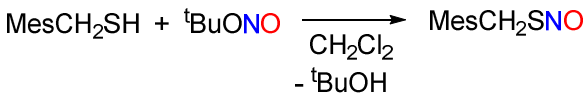

Scheme S2. Synthesis of $MesCH_2SNO$.

^{t}BuONO (0.744 g, 7.216 mmol) was directly added to a solution of $MesCH_2SH$ (0.3 g, 1.804 mmol) in dichloromethane at -40 °C (*ca.* 3 mL). The solution was stirred for 10 min at RT and the resultant dark pink solution was dried to obtain dark pink oil (0.31 g, 1.587 mmol) in 88% yield.

^{1}H NMR (400 MHz, 298 K, $CDCl_3$): δ 6.83 (s, 2H, Aryl-CH), 4.70 (s, 2H, C*H*$_2$), 2.25 (s, 3H, CH_3), 2.16 (s, 6H, CH_3) (Figure S6).

$^{13}C\{^{1}H\}$ NMR (100 MHz, 298 K, $CDCl_3$): *δ* 137.36, 137.03, 129.28, 129.22, 32.15, 20.98, 19.94.

^{15}N NMR (41 MHz, -60 °C, CD_2Cl_2): δ 821.50 (s, *anti*, $MesCH_2S^{15}NO$), δ 756.10 (s, *syn*, $MesCH_2S^{15}NO$). ^{15}N NMR (41 MHz, 10 °C, CD_2Cl_2): δ 764.823 (s, *syn*, $MesCH_2S^{15}NO$) (Figure S7).

UV-Vis (CH_2Cl_2, 25 °C): λ_{max}/nm (ε/$M^{-1}cm^{-1}$) = 549 (52), 517 (21) (Figure S8).

FT-IR (cm^{-1}): 1484 ν(^{14}NO); 630 ν(S-^{14}N); 1461 ν(^{15}NO); 614 ν(S-^{15}N); Hooke's law predicts $^{15N/14N}\Delta\nu$ = 27 cm^{-1} and $^{15N/14N}\Delta\nu$ = 16, respectively (Figure S9). The IR spectra were taken by putting $MesCH_2SNO$ as a dense oil directly on the ATR instrument.

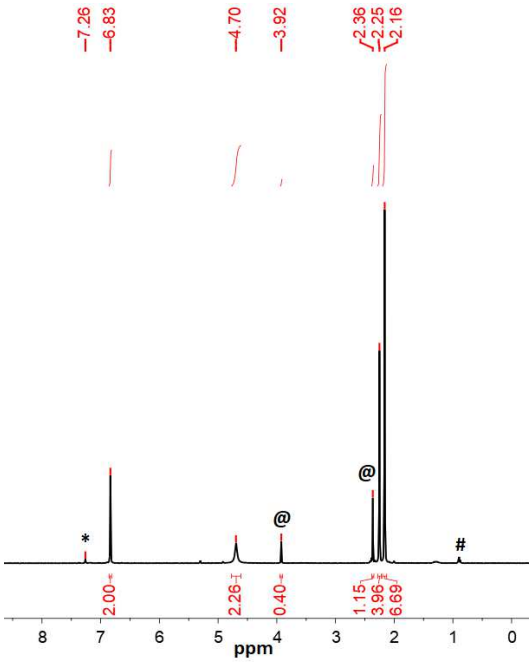

Figure S6. ^{1}H NMR spectrum (400 MHz, 25 °C, $CDCl_3$) of $MesCH_2SNO$ (**2**). The resonances marked with (*) and (#) are from the solvent residual peak for chloroform-d_1 and pentane, respectively. The resonances marked with (@) is from $MesCH_2SSCH_2Mes$ formed due to the decomposition of $MesCH_2SNO$.

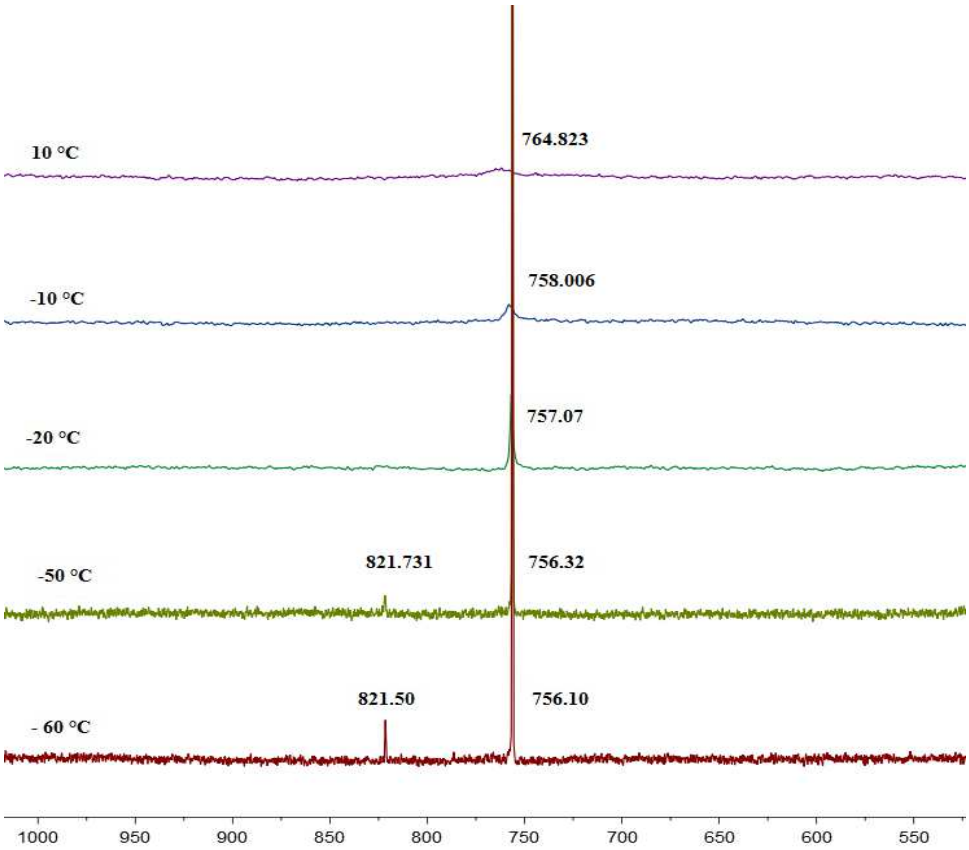

Figure S7. Variable temperature ^{15}N NMR spectra (41 MHz, CD_2Cl_2) of $MesCH_2S^{15}NO$ (**2-^{15}N**).

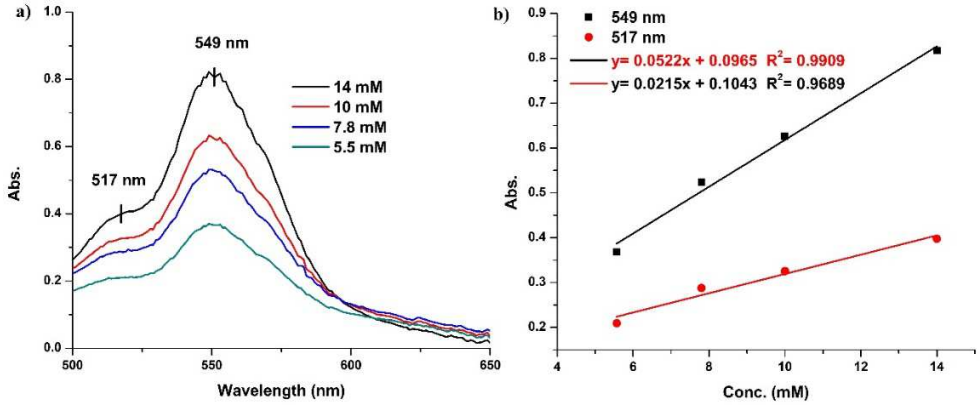

Figure S8. a) UV-Vis spectra of $MesCH_2SNO$ (**2**) in dichloromethane at 25 °C at different concentrations. b) Beer's law plot for (**2**) depicts λ_{max} = 517 nm (ε =21 $M^{-1}cm^{-1}$) and λ_{max} = 549 nm (ε = 52 $M^{-1}cm^{-1}$).

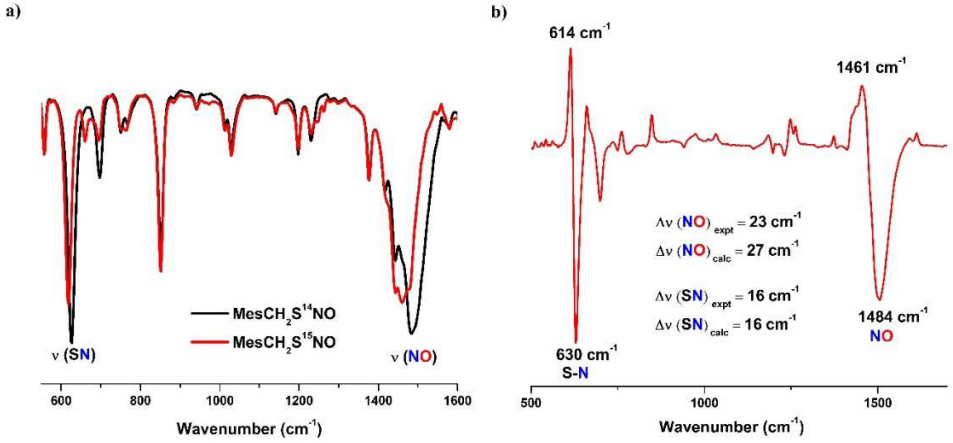

Figure S9. a) FT-IR spectra of $MesCH_2S^{14}NO$ (**2**) (black trace) and $MesCH_2S^{15}NO$ (**2**-^{15}**N**) (red trace). b) The difference spectrum between (**2**) (down) and (**2**-^{15}**N**) (up).

5. Synthesis and Characterization of AdSNO-B(C_6F_5)$_3$ (3)

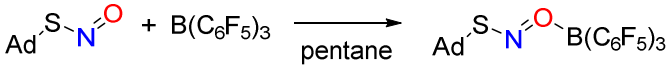

Scheme S3. Synthesis of AdSNO-B(C_6F_5)$_3$ (**3**).

A solution of B(C_6F_5)$_3$ (0.259 g, 0.506 mmol) in pentane (5 mL) was added to a solution of AdSNO (0.1 g, 0.506 mmol) in pentane (2 mL). The color of the solution immediately changed from dark green to yellow. The solution was concentrated to ca. 3 mL and kept at -40 °C to give the product (0.29 g, 80% yield) as yellow color crystals.

^{1}H NMR (400 MHz, 298 K, $CDCl_3$): δ 2.35 (d, 6H, CH_2), 2.29 (m, 3H, C*H*), 1.87 (d, 6H, CH_2) (Figure S10).

^{19}F NMR (376 MHz, 298 K, $CDCl_3$): δ -131.36 (m, 6F), -151.38 (m, 3F), -162.45 (m, 6F) (Figure S11).

^{13}C{^{1}H} NMR (100 MHz, 233.15 K, $CDCl_3$): δ 147.72 (m), 140.64 (m), 137.68 (m), 114.93 (m), 65.53, 42.76(minor), 42.08(major), 37.04(minor), 35.89(minor), 35.30(minor), 35.05(major), 29.76(minor), 29.52(major), 29.03(minor) (Figure S12).

^{15}N NMR (41 MHz, -60 °C, CD_2Cl_2): δ 740.59 (s, *O-anti*-AdS^{15}NO-B(C_6F_5)$_3$), 681.25 (s, *O-syn*-AdS^{15}NO-B(C_6F_5)$_3$), 553.49 (s, *N-syn*-AdS^{15}NO-B(C_6F_5)$_3$) (Figure S13).

UV-Vis (CH_2Cl_2, 25 °C): λ_{max}/nm (ε/M^{-1}cm^{-1}) = 510 (9) (Figure S15).

FT-IR (X, cm^{-1}): 1257 ν(^{14}NO); 853 ν(S-^{14}N); 1237 ν(^{15}NO); 835 ν(S-^{15}N); Hooke's law predicts $^{15N/14N}\Delta\nu$ = 24 cm^{-1} and $^{15N/14N}\Delta\nu$ = 20, respectively (Figure S16). The IR spectra were taken by putting AdSNO-B(C_6F_5)$_3$ as a fine powder directly on the ATR instrument. Anal. Calcd for $C_{28}H_{15}BF_{15}NOS$ (**3**): C, 47.42; H, 2.13; N, 1.97. Found: C, 47.55; H, 2.48; N, 1.34. The lower experimental value for N arises from loss of NO from AdSNO-BCF due to its thermal instability.

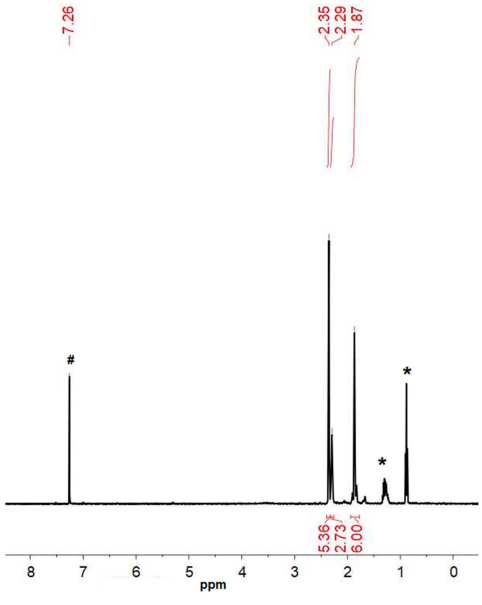

Figure S10. ^{1}H NMR spectrum (400 MHz, 25 °C, $CDCl_3$) of AdSNO-BCF (**3**). The resonances marked with (*) and (#) are from the solvent residual peak pentane and chloroform-d_1, respectively.

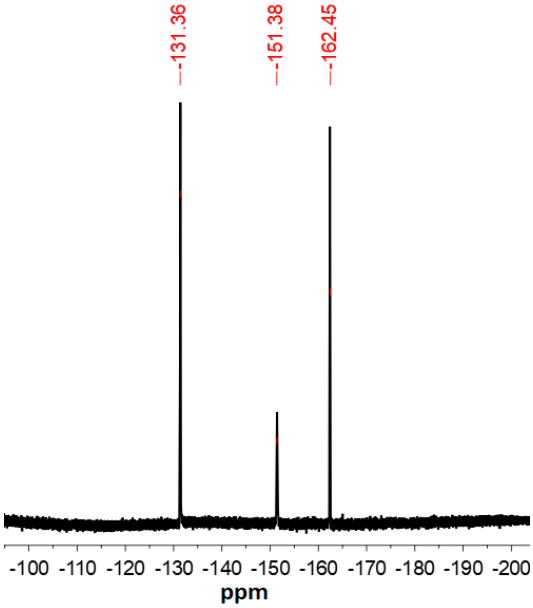

Figure S11. ^{19}F NMR spectrum (376 MHz, 25 °C, $CDCl_3$) of AdSNO-BCF (**3**).

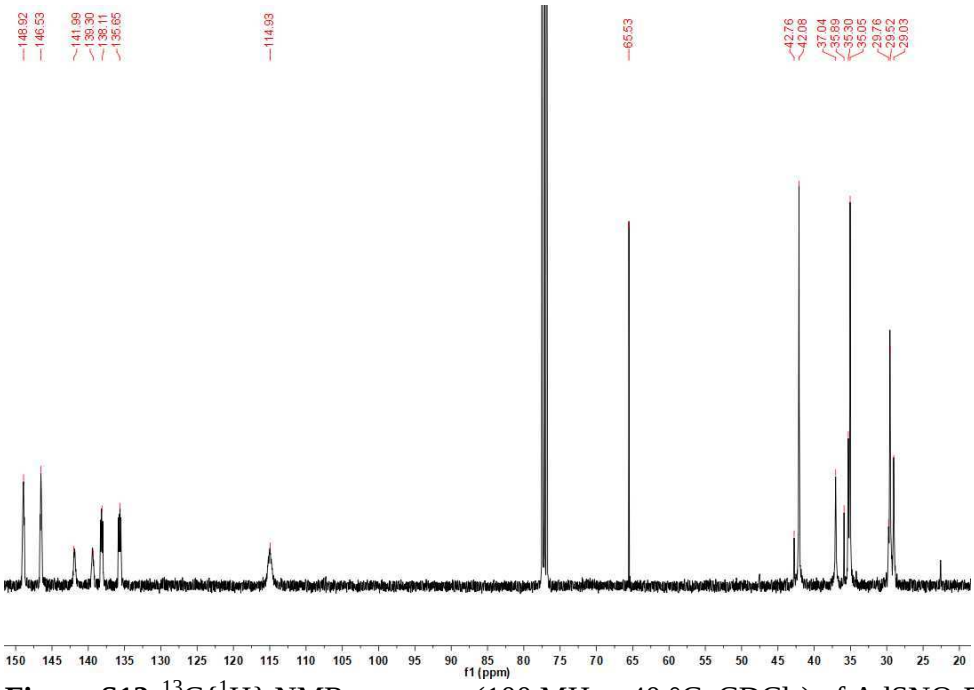

Figure S12. ^{13}C{^{1}H} NMR spectrum (100 MHz, -40 °C, $CDCl_3$) of AdSNO-BCF (**3**).

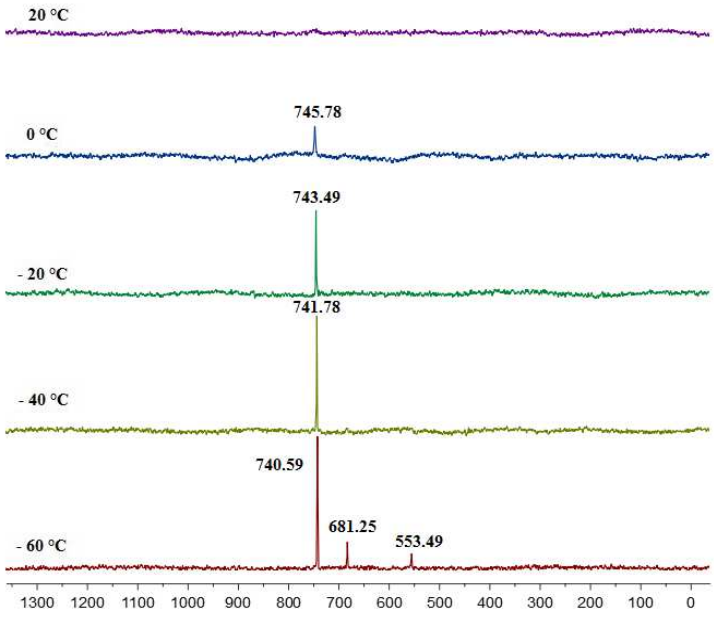

Figure S13. Variable temperature ^{15}N NMR spectra (41 MHz, CD_2Cl_2) of Ad$S^{15}NO$-$B(C_6F_5)_3$ (**3-^{15}N**).

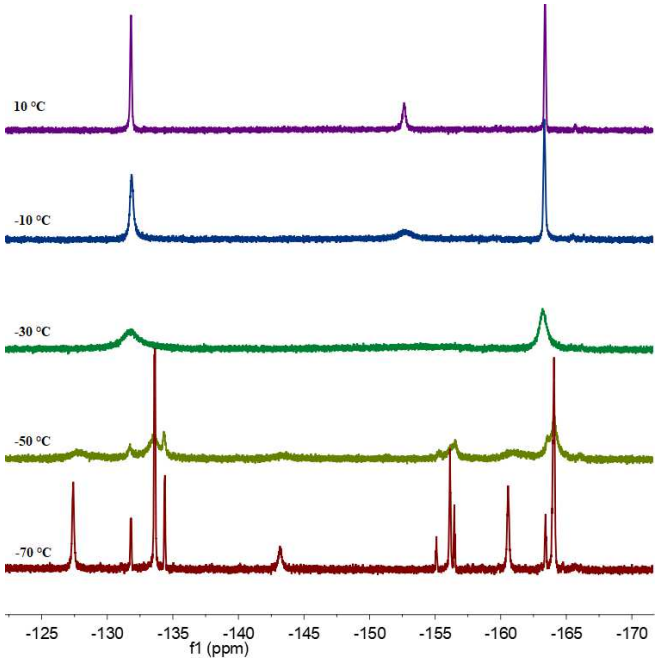

Figure S14. Variable temperature ^{19}F NMR spectra (376 MHz, CD_2Cl_2) of Ad$S^{15}NO$-$B(C_6F_5)_3$ (**3-^{15}N**).

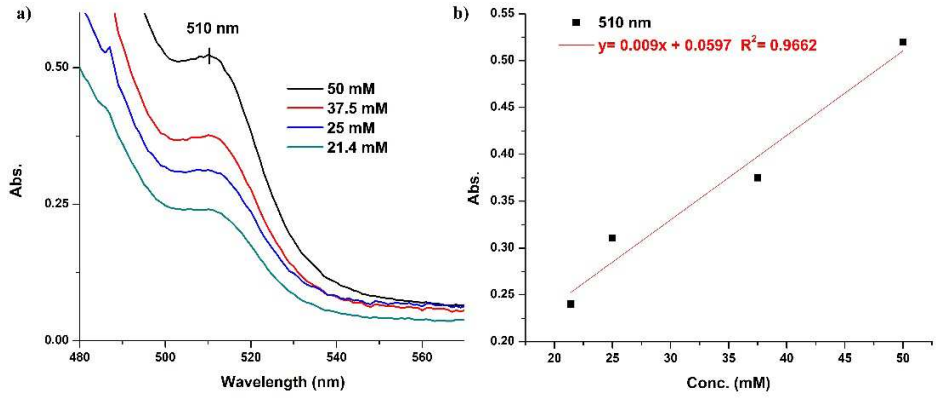

Figure S15. a) UV-Vis spectra of AdSNO-B(C_6F_5)$_3$ (**3**) in dichloromethane at 25 °C at different concentrations. b) Beer's law plot for (**3**) depicts λ_{max} = 510 nm (ε = 9 $M^{-1}cm^{-1}$).

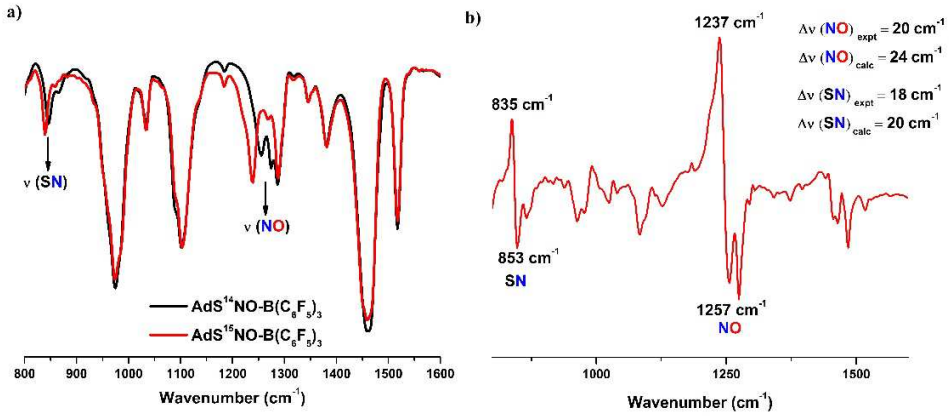

Figure S16. a) FT-IR spectra of AdS^{14}NO-B(C_6F_5)$_3$ (**3**) (black trace) and AdS^{15}NO-B(C_6F_5)$_3$ (**3**-^{15}**N**) (red trace). b) The difference spectrum between (**3**) (down) and (**3**-^{15}**N**) (up).

6. Synthesis and Characterization of $MesCH_2SNO$-$B(C_6F_5)_3$ (4)

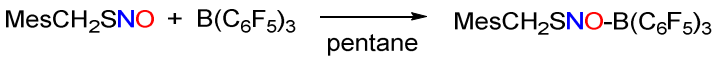

Scheme S4. Synthesis of $MesCH_2SNO$-$B(C_6F_5)_3$ (**4**).

A solution of $B(C_6F_5)_3$ (0.262 g, 0.512 mmol) in pentane (5 mL) was added to a solution of $MesCH_2SNO$ (0.1 g, 0.512 mmol) in pentane (2 mL). The color of the solution immediately changed from pink to orange. The solution was concentrated to ca. 3 mL and kept at -40 °C to yield to give the product (0.26 g, 71% yield) as orange crystals.

^{1}H NMR (400 MHz, 298 K, $CDCl_3$): δ 6.87 (s, 2H, Aryl-CH), 4.79 (s, 2H, C*H*$_2$), 2.26 (s, 3H, CH_3), 2.18 (s, 6H, CH_3) (Figure S17).

^{19}F NMR (376 MHz, 298 K, $CDCl_3$): δ -129.93 (m, 6F), -148.16 (m, 3F), -161.36 (m, 6F) (Figure S18).

^{13}C{^{1}H} NMR (100 MHz, 233.15 K, $CDCl_3$): *δ* 147.81 (m), 140.44(s), 140.81 (m), 138.45(s), 137.01(m), 130.08(s), 118.19(s), 114.69(m), 41.48(s), 21.21(s, minor), 21.21(s, major), 20.16(s, minor), 20.09(s, major) (Figure S19).

^{15}N NMR (41 MHz, -70 °C, CD_2Cl_2): δ 678.24 (s), 553.97 (s), 231.756 (s) (Figure S20).

UV-Vis (CH_2Cl_2, 25 °C): λ_{max}/nm (ε/$M^{-1}cm^{-1}$) = 481 (40) (Figure S22).

FT-IR (X, cm^{-1}): 1282 ν(^{14}NO); 863 ν(S-^{14}N); 1261 ν(^{15}NO); 845 ν(S-^{15}N); Hooke's law predicts $^{15N/14N}\Delta\nu$ = 25 cm^{-1} and $^{15N/14N}\Delta\nu$ = 20, respectively (Figure S23). The IR spectra were taken by putting $MesCH_2SNO$-$B(C_6F_5)_3$ as a fine powder directly on the ATR instrument.

Anal. Calcd for $C_{28}H_{13}BF_{15}NOS$ (**4**): C, 47.55; H, 1.85; N, 1.98. Found: C, 47.58; H, 2.08; N, 1.05. The lower experimental value for N arises from loss of NO from $MesCH_2SNO$-BCF due to its thermal instability.

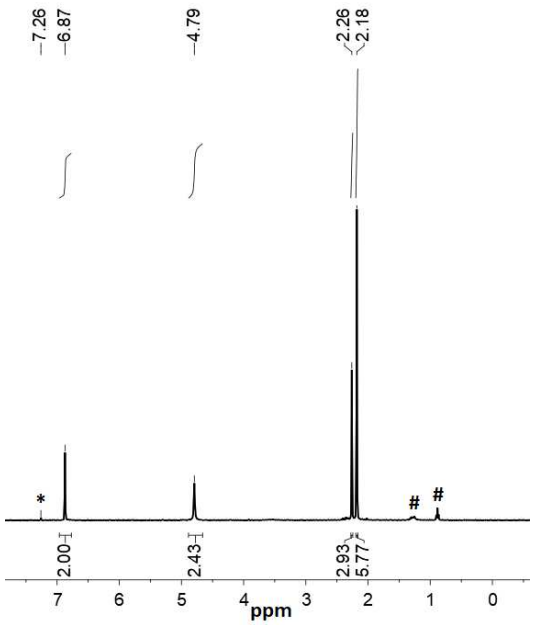

Figure S17. ^{1}H NMR spectrum (400 MHz, 25 °C, $CDCl_3$) of $MesCH_2SNO$-BCF (**4**). The resonances marked with (*) and (#) are from the solvent residual peak for chloroform-d_1 and pentane, respectively.

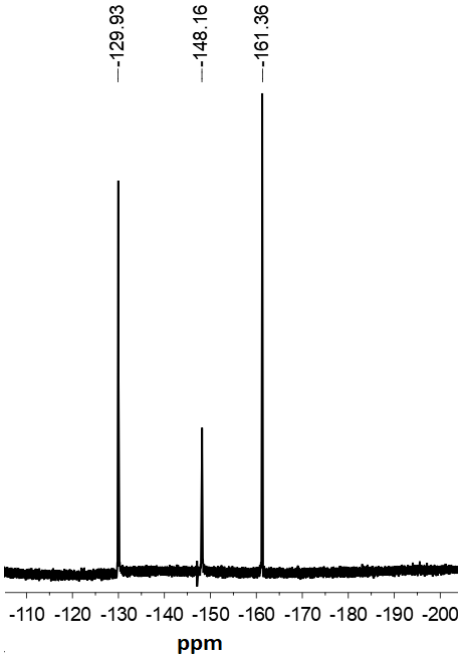

Figure S18. ^{19}F NMR spectrum (376 MHz, 25 °C, $CDCl_3$) of $MesCH_2SNO$-BCF (**4**).

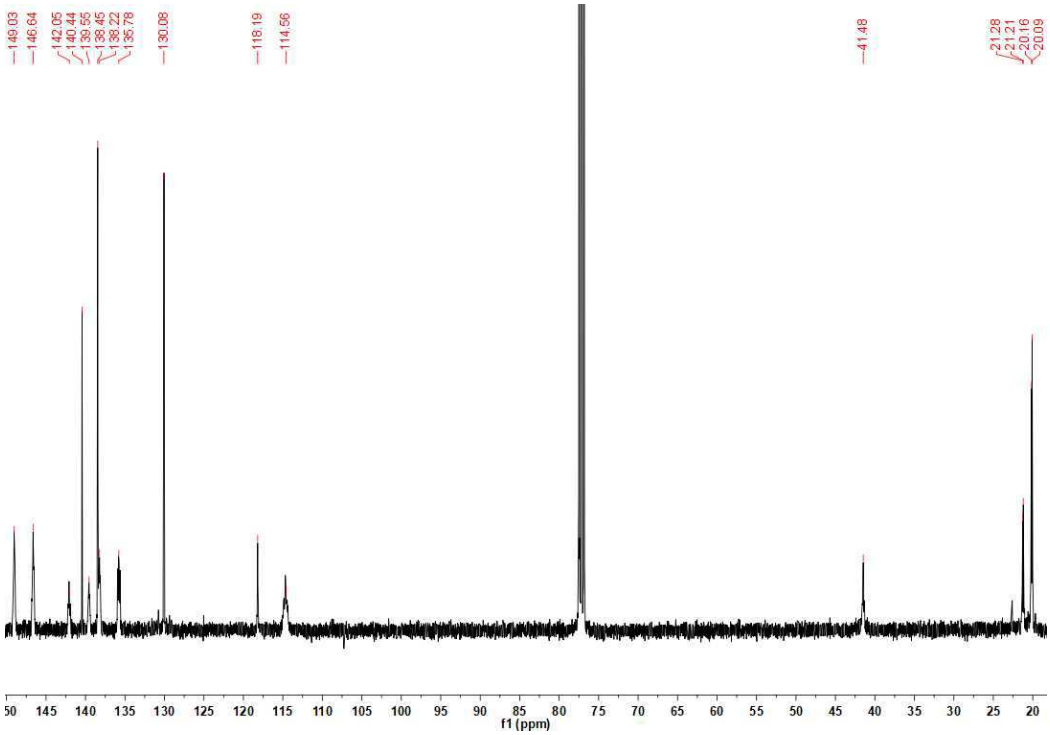

Figure S19. $^{13}C\{^{1}H\}$ NMR spectrum (100 MHz, -40 °C, $CDCl_3$) of $MesCH_2SNO$-BCF (**4**).

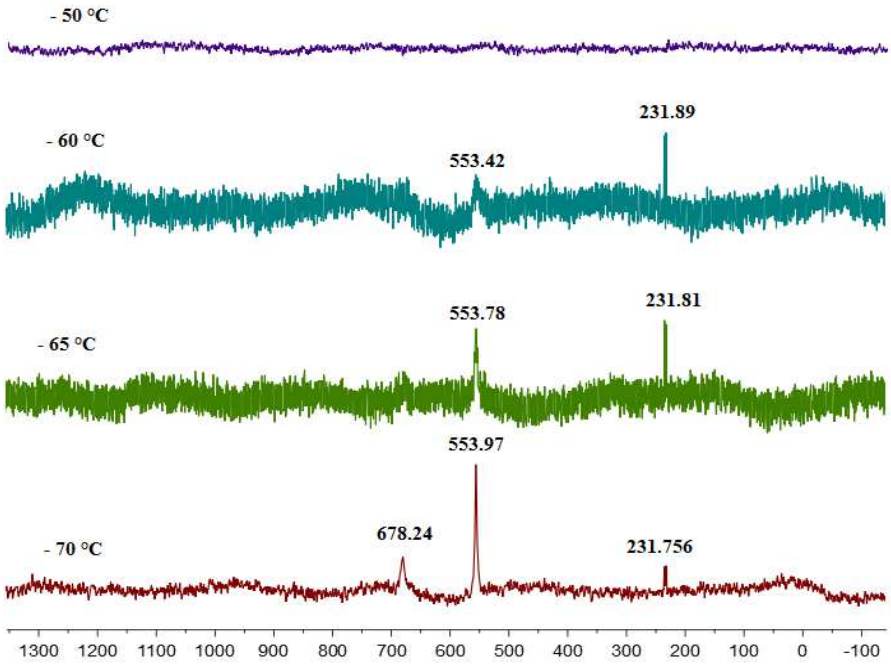

Figure S20. Variable temperature ^{15}N NMR spectra (41 MHz, CD_2Cl_2) of $MesCH_2S^{15}NO\text{-}B(C_6F_5)_3$ (**4**-^{15}**N**).

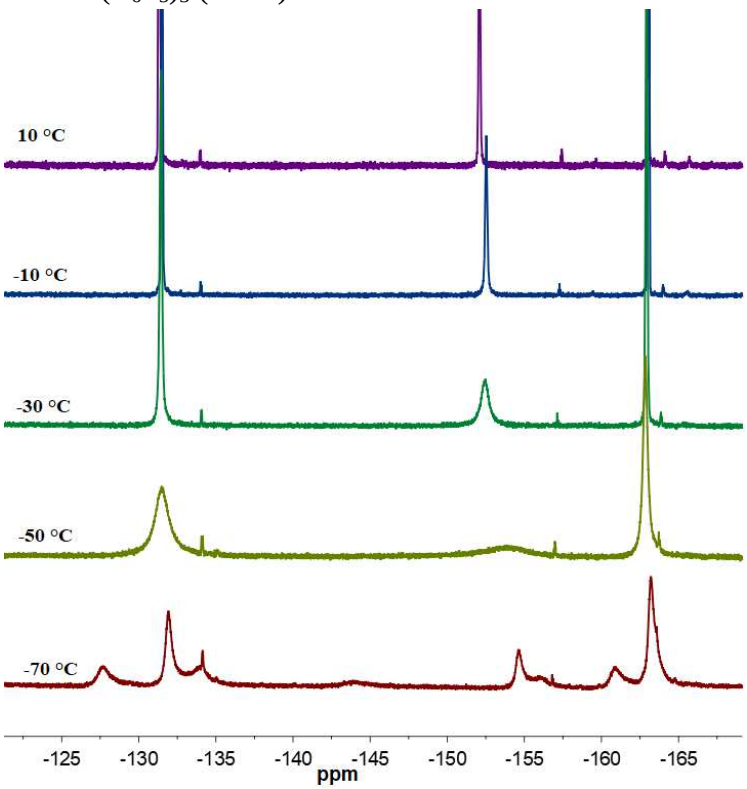

Figure S21. Variable temperature ^{19}F NMR spectra (376 MHz, CD_2Cl_2) of $MesCH_2SNO\text{-}BCF$ (**4**).

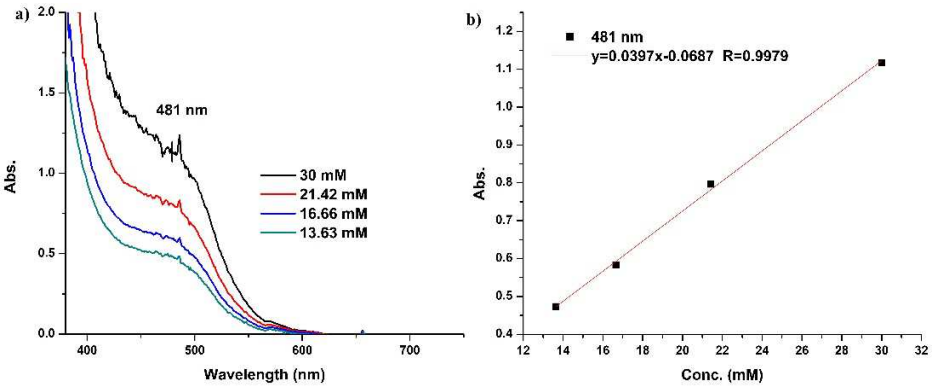

Figure S22. a) UV-Vis spectra of $MesCH_2SNO\text{-}B(C_6F_5)_3$ (**4**) in dichloromethane at 25 °C at different concentrations. b) Beer's law plot for (**4**) depicts λ_{max}/nm (ε/$M^{-1}cm^{-1}$) = 481 (40).

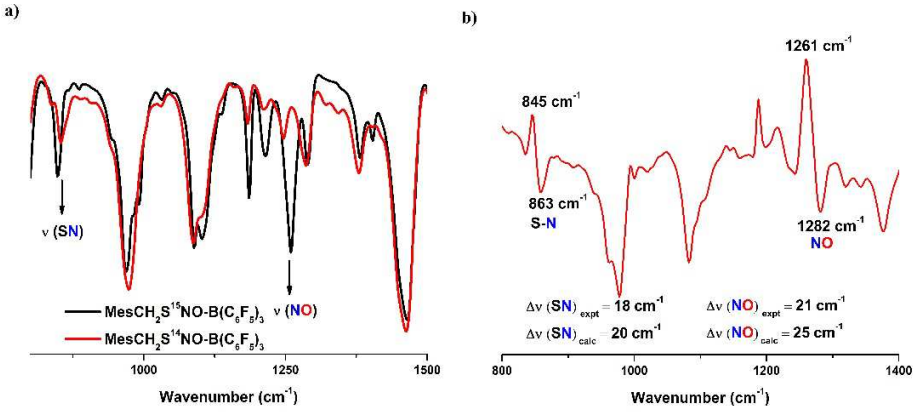

Figure S23. a) FT-IR spectra of $MesCH_2S^{14}NO$ (**4**) (red trace) and $MesCH_2S^{15}NO$ **(4-^{15}N)** (black trace). b) The subtracted spectrum of (**4**) (down) and (**4-^{15}N**) (up).

7. Cyclic Voltammetry Measurements

General Considerations. Cyclic voltammetry measurements were done at room temperature under dry nitrogen atmosphere of a glove-box using a BASi Epsilon Electrochemistry setup with three electrodes (Working electrode: glassy carbon, Auxiliary electrode: platinum wire, Pseudo-reference electrode: silver/silver nitrate). As a non-coordinating electrolyte tetrabutylammonium teraphenylborate was used for all cyclic voltammetry measurements.

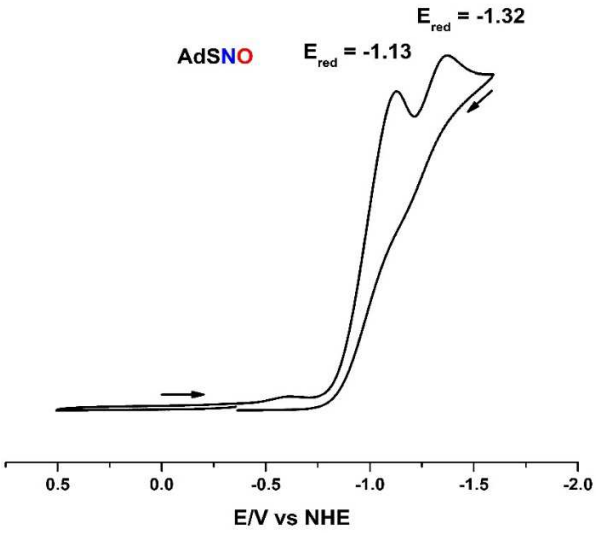

Figure S24. Cyclic voltammetry of Ad-SNO (**1**) (7 mM) in dichloromethane at 25 °C in presence of $[Bu_4N][BPh_4]$ (0.1 M) with the scan rate of 50 mV/s.

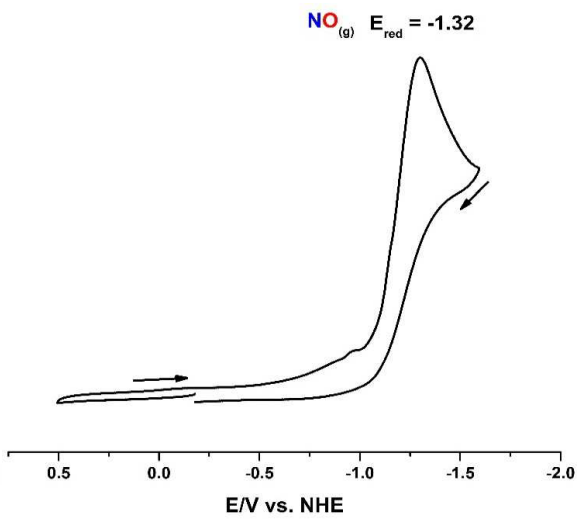

Figure S25. Cyclic voltammetry of NO gas (saturated solution) in dichloromethane at 25 °C in presence of $[Bu_4N][BPh_4]$ (0.1 M).

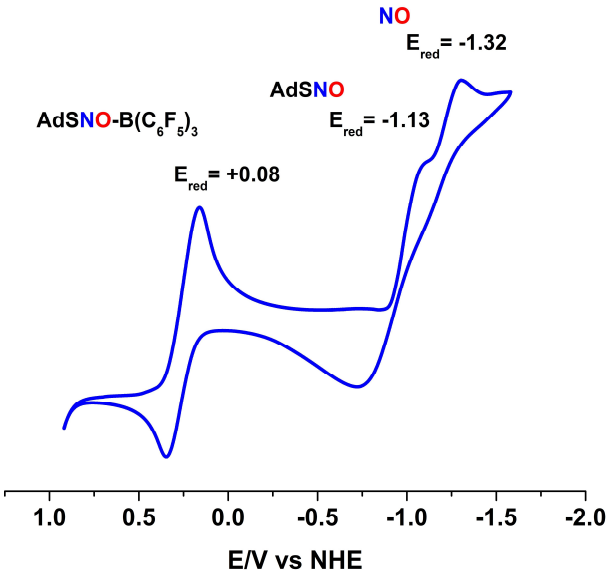

Figure S26. Cyclic voltammogram of AdSNO-$B(C_6F_5)_3$ (**3**) (7 mM) in dichloromethane at 25 °C with a scan rate of 50 mV/s in the presence of $[Bu_4N][BPh_4]$ (0.1 M). Reduction of free AdSNO and free NO are observed at -1.13 V and -1.32 V, respectively. This suggests the presence of free $B(C_6F_5)_3$ that has been reported at -1.09 V* which may overlap with the free AdSNO wave.

*E. J. Lawrence, V. S. Oganesyan, G. G. Wildgoose, A. E. Ashley. *Dalton Trans.* **2013**, *42*, 782-789.

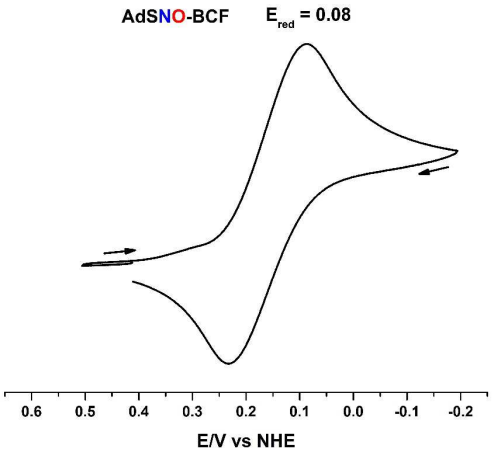

Figure S27a. Cyclic voltammetry of AdSNO-$B(C_6F_5)_3$ (**3**) (7 mM) in dichloromethane at 25 °C in presence of $[Bu_4N][BPh_4]$ (0.1 M) with the scan rate of 50 mV/s.

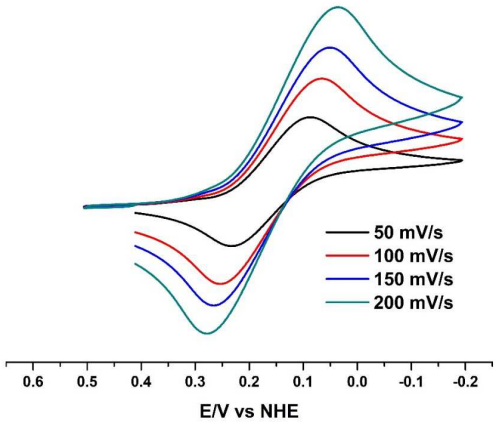

Figure S27b. Cyclic voltammetry of AdSNO-$B(C_6F_5)_3$ (**3**) (7 mM) in dichloromethane at 25 °C in presence of $[Bu_4N][BPh_4]$ (0.1 M) at different scan rates.

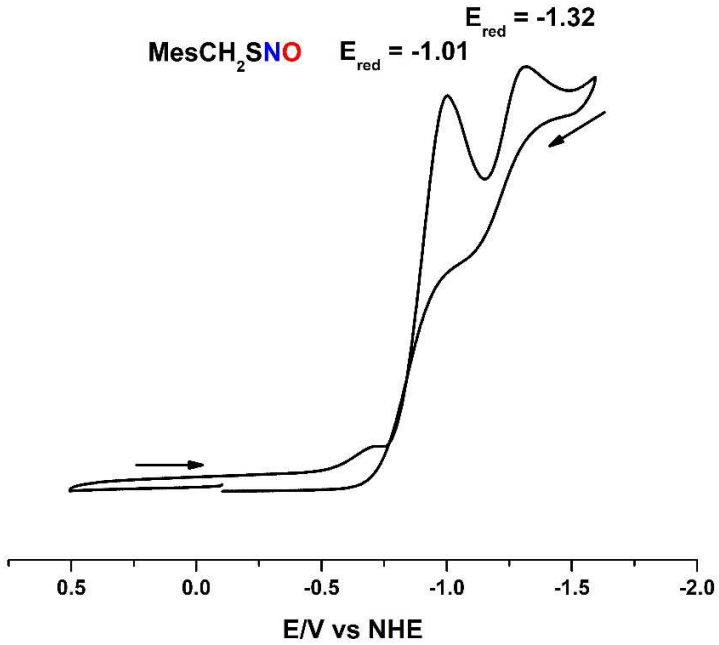

Figure S28. Cyclic voltammetry of $MesCH_2SNO$ (**2**) (7 mM) in dichloromethane at 25 °C in presence of $[Bu_4N][BPh_4]$ (0.1 M) with the scan rate of 50 mV/s.

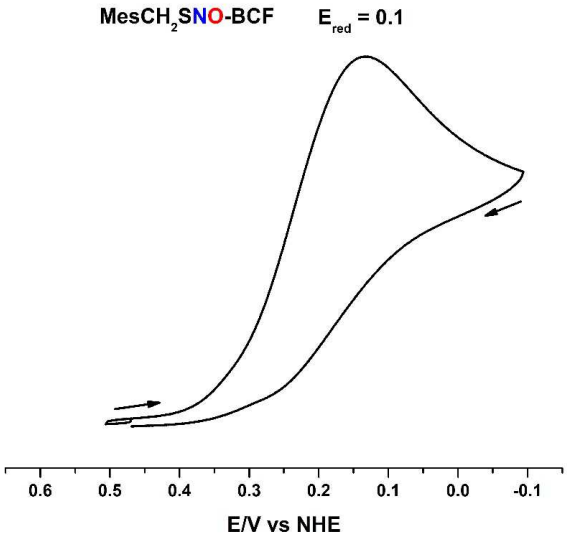

Figure S29. Cyclic voltammetry of $MesCH_2SNO\text{-}B(C_6F_5)_3$ (**4**) (7 mM) in dichloromethane at 25 °C in presence of $[Bu_4N][BPh_4]$ (0.1 M) with the scan rate of 50 mV/s.

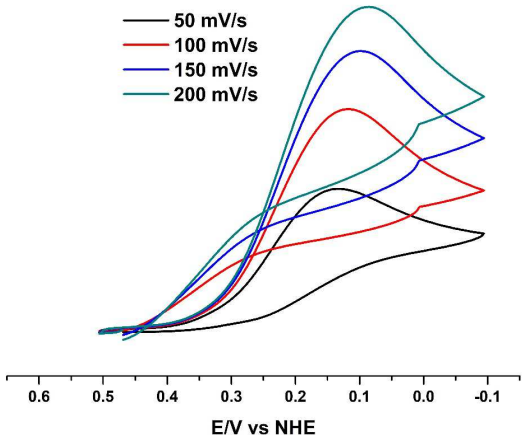

Figure S30. Cyclic voltammetry of $MesCH_2SNO\text{-}B(C_6F_5)_3$ (**4**) (7 mM) in dichloromethane at 25 °C in presence of $[Bu_4N][BPh_4]$ (0.1 M) at different scan

8. Reduction of AdSNO (1) with Cp^*_2Co

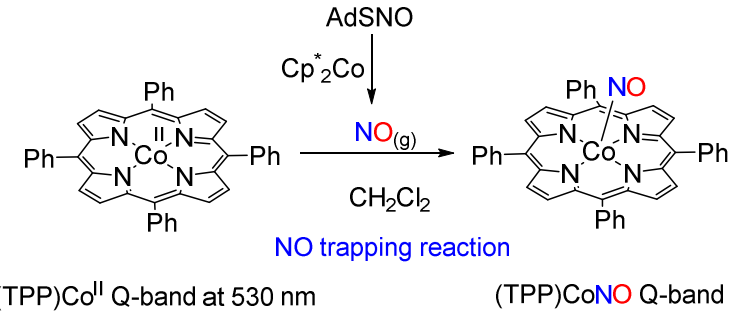

Scheme 5. Trapping NO released from reaction of AdSNO (**1**) with Cp^*_2Co by $(TPP)Co^{II}$.

Quantitative trapping of nitric oxide was done using Cobalt(II)-meso-tetraphenylporphine [$(TPP)Co^{II}$] which was purchased from Strem Chemical and used for a similar experimental set up as previously described.[3]AdSNO (**1**) (1.0 mL, 10.0 mM) was weighed in a small vial and placed in a larger vial. The lager vial was sealed with a septum. A solution of $(TPP)Co^{II}$ complex (10.0 mL, 1.0 mM) in dichloromethane was injected to the big vial. Then a solution of decamethylcobaltocene (1.0 mL, 10.0 mM) in fluorobenzene was injected to the inner vial and the solutions in both vials stirred for 1 hr. Then an aliquot (100 μL) of the resultant (TPP)Co solution from outer vial was diluted to 2.0 mL using CH_2Cl_2 and analyzed by UV-Vis spectroscopy. The Q-band absorption features in the UV-Vis spectra of authentic $(TPP)Co^{II}$ (530 nm) and (TPP)Co(NO) (540 nm) samples were used to compare and quantify the yield of cobalt-nitrosyl species.

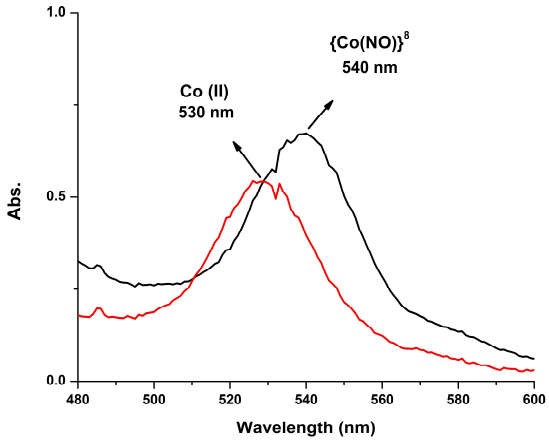

Figure S31. UV-Vis spectra (in CH_2Cl_2 at 25 °C) of (TPP)Co (red trace) and (TPP)Co(NO) (black trace) species generated from the reaction of $(TPP)Co^{II}$ with NO released from the reaction of AdSNO (**1**) with Cp^*_2Co. The yield of NO formation is 82%.

9. Reduction of $MesCH_2SNO$ (2) with Cp^*_2Co

Decamethylcobaltocene (1.0 mL 10.0 mM) in fluorobenzene was added to $MesCH_2SNO$ (**2**) (1 mL, 10 mM) in fluorobenzene and the solution stirred for 5 h. Formation of NO from the reaction of $MesCH_2SNO$ (**2**) and decamethylcobaltocene was quantitatively measured by employing $(TPP)Co^{II}$ complex as a NO trap in 71% yield.

10. Reduction of AdSNO-$B(C_6F_5)_3$ (3) with Cp^*_2Co

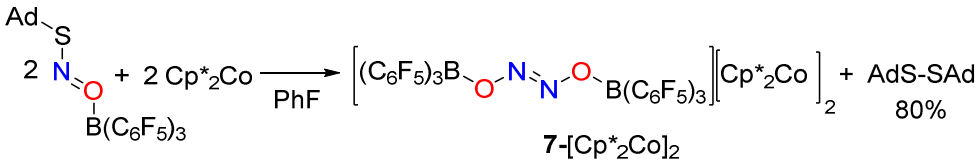

Scheme S6. Reduction of AdSNO-BCF (**3**) with Cp^*_2Co.

A solution of decamethylcobaltocene (0.046 g, 0.141 mmol) in fluorobenzene (3 mL) was added to a solution of AdSNO-BCF (**3**) (0.1 g, 0.141 mmol) in fluorobenzene (2 mL). The color of the solution immediately changed from yellow to dark yellow. The solution was evaporated, and the resulting dark yellow solid was washed with pentane. The solid was then dissolved in 3 mL dichloromethane and was layered with cold pentane and kept at -40 °C to give the product $[(C_6F_5)_3B\text{-}ON{=}NO\text{-}B(C_6F_5)_3][Cp^*_2Co]_2$ (**7**-$[Cp^*_2Co]_2$) (0.180 g, 73% yield) as yellow crystals. ^1H NMR analysis on the yellow solution indicates the formation of free disulfide in 80% yield via its ^1H NMR spectrum (400 MHz, 298 K, $CDCl_3$): δ 2.06 (br, 6H, CH_2-Ad), 1.82 (br, 12H, CH_2-Ad), 1.67 (br, 12H, CH_2-Ad).

Characterization data for **7**-$[Cp^*_2Co]_2$

^1H NMR (400 MHz, 298 K, $CDCl_3$): δ 1.60 (s, 30H) (Figure S32).

$^{13}C\{^1H\}$ NMR (100 MHz, 233.15 K, CD_2Cl_2): δ 147.69 (m), 138.42 (m), 136.11 (m), 123.28(m), 93.84, 7.87.

^{19}F NMR (376 MHz, 298 K, $CDCl_3$): δ -132.29 (m, 6F), -163.57 (m, 3F), -167.17 (m, 6F) (Figure S33).

^{15}N NMR (41 MHz, -40 °C, CD_2Cl_2): δ 429.91, δ 384.93 (Figure S34).

UV-Vis (CH_2Cl_2, 25 °C): λ_{max}/nm (ε/$M^{-1}cm^{-1}$) = 340 (1575), 405 (344) (Figure S35).

FT-IR (X, cm^{-1}): 1010 $\nu(^{14}NO)$; 987 $\nu(^{15}NO)$; Hooke's law predicts $^{15N/14N}\Delta\nu$ = 19 cm^{-1} (Figure S36). The IR spectra were taken as a thin film by evaporating a dichloromethane solution of **7**-$[Cp^*_2Co]_2$ on a KBr window.

Anal. Calcd for $C_{76}H_{60}B_2Co_2F_{30}N_2O_2$ (**7**-$[Cp^*_2Co]_2$): C, 52.38; H, 3.47; N, 1.61. Found: C, 52.22; H, 3.49; N, 1.55.

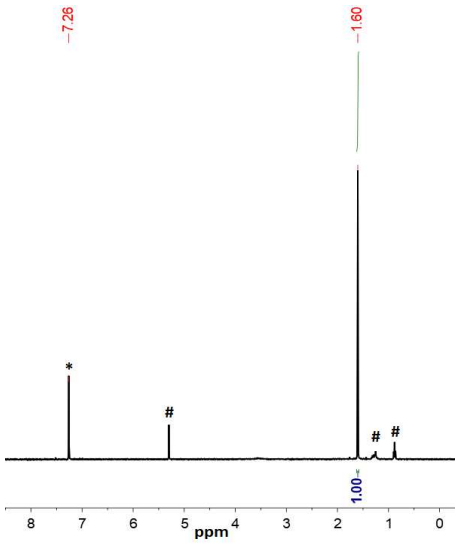

Figure S32. ^1H NMR spectrum (400 MHz, 25 °C, $CDCl_3$) of $[(C_6F_5)_3B\text{-}ON{=}NO\text{-}B(C_6F_5)_3][Cp^*_2Co]_2$ (**7**-$[Cp^*_2Co]_2$). The resonances marked with (*) and (#) are from the solvent residual peak for chloroform-d_1 and pentane, respectively.

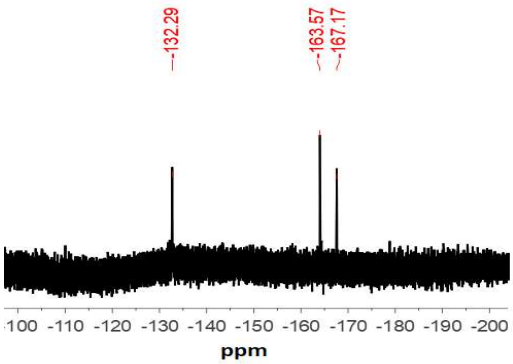

Figure S33. ^{19}F NMR spectrum (376 MHz, 25 °C, $CDCl_3$) of $[(C_6F_5)_3B\text{-}ON{=}NO\text{-}B(C_6F_5)_3][Cp^*_2Co]_2$ (**7**-$[Cp^*_2Co]_2$).

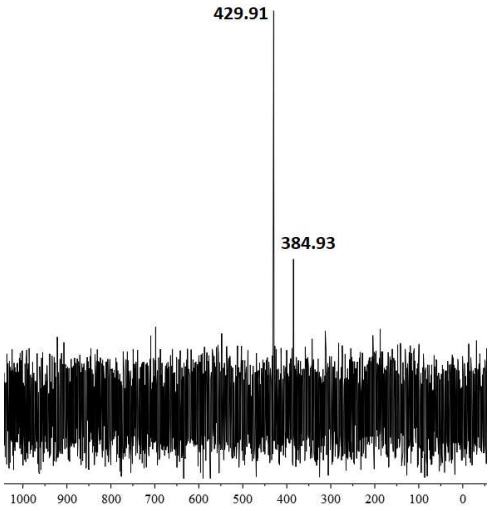

Figure S34. ^{15}N NMR spectrum (41 MHz, CD_2Cl_2) of $[(C_6F_5)_3B\text{-}ON{=}NO\text{-}B(C_6F_5)_3][Cp^*_2Co]_2$ (**7**-$[Cp^*_2Co]_2$) at -

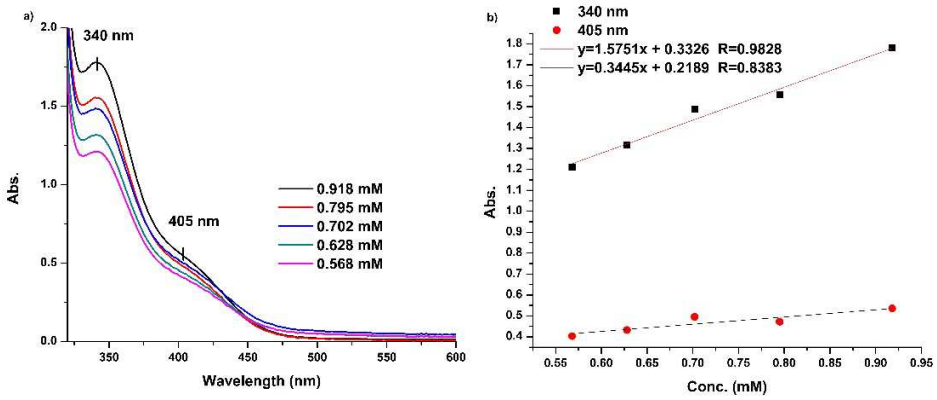

Figure S35. a) UV-Vis spectra of $[(C_6F_5)_3B\text{-}ON{=}NO\text{-}B(C_6F_5)_3][Cp^*_2Co]_2$ at 25 °C (**7**-$[Cp^*_2Co]_2$) in dichloromethane at 25 °C at different concentrations. b) Beer's law plot for (**7**-$[Cp^*_2Co]_2$) depicts λ_{max}/nm (ε/$M^{-1}cm^{-1}$) = 340 (1575).

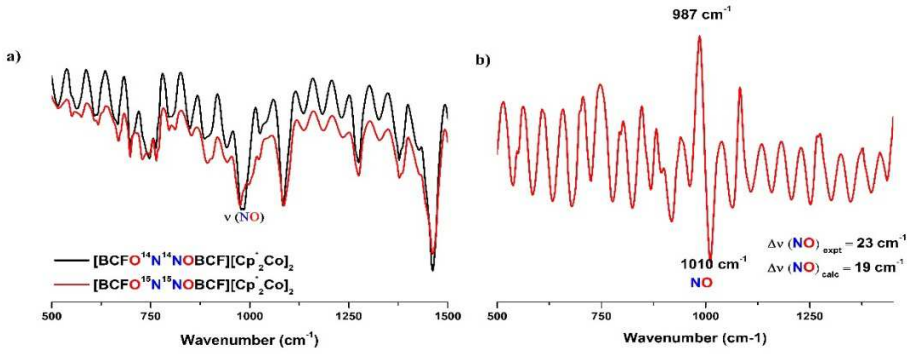

Figure S36. a) FT-IR spectra of $[(C_6F_5)_3B\text{-}O^{14}N{=}^{14}NO\text{-}B(C_6F_5)_3][Cp_2{}^*Co]_2$ (**7**-$[Cp^*_2Co]_2$) (black trace) and $[(C_6F_5)_3B\text{-}O^{15}N{=}^{15}NO\text{-}B(C_6F_5)_3][Cp^*_2Co]_2$ (**7**-$[Cp^*_2Co]_2$-**^{15}N**) (red trace). b) The subtracted spectrum of (**7**-$[Cp^*_2Co]_2$) (down) and (**7**-$[Cp^*_2Co]_2$-**^{15}N**) (up).

11. Reduction of $MesCH_2SNO$-BCF (4) with Cp^*_2Co

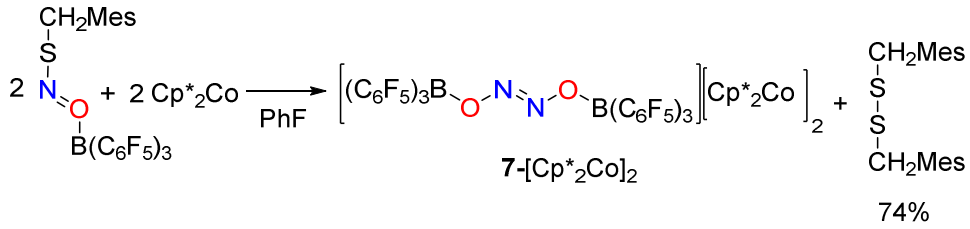

Scheme S7. Reduction of $MesCH_2SNO$-BCF (**4**) with Cp^*_2Co.

A solution of decamethylcobaltocene (0.046 g, 0.141 mmol) in fluorobenzene (3 mL) was added to a solution of $MesCH_2SNO$-BCF (**4**) (0.1 g, 0.141 mmol) in fluorobenzene (2 mL). The color of the solution immediately changed from orange to dark yellow. The solution was evaporated, and the resulting dark yellow solid was washed with pentane. The solid was then dissolved in 3 mL dichloromethane and filtered through celite to give a clear solution which was layered with cold pentane and kept at -40 °C to give the product $[(C_6F_5)_3B\text{-}O^{15}N=^{15}NO\text{-}B(C_6F_5)_3][Cp^*_2Co]_2$ (**7**-$[Cp^*_2Co]_2$) (0.160 g, 65% yield) as yellow crystals. ^{1}H NMR analysis on the yellow solution indicates the formation of free disulfide in 74% yield via its ^{1}H NMR spectrum (400 MHz, 298 K, $CDCl_3$): δ 6.83 (s, 2H, Aryl-CH), 3.92 (s, 2H, CH_2), 2.36 (s, 3H, CH_3), 2.24 (s, 6H, CH_3).

Reduction of AdSNO-$B(C_6F_5)_3$ (3) with Cp_2Fe

A solution of ferrocene (0.026 g, 0.141 mmol) in dichloromethane (3 mL) was added to a solution of AdSNO-BCF (**3**) (0.1 g, 0.141 mmol) in dichloromethane (2 mL). The color of the solution immediately changed from yellow to purple. The solution was evaporated, and the resulting purple solid was washed with pentane. The solid was then dissolved in 3 mL fluorobenzene and was layered with cold pentane and kept at -40 °C to give the product $[(C_6F_5)_3B\text{-}ON=NO\text{-}B(C_6F_5)_3][Cp_2Fe]_2$ (**7**-$[Cp_2Fe]_2$) (0.145 g, 70% yield) as purple crystal.

Scheme S8. Reduction of AdSNO-BCF (**3**) with Cp_2Fe.

13. Reduction of $MesCH_2SNO\text{-}B(C_6F_5)_3$ (4) with Cp_2Fe

A solution of ferrocene (0.026 g, 0.141 mmol) in dichloromethane (3 mL) was added to a solution of $MesCH_2SNO$-BCF (**4**) (0.1 g, 0.141 mmol) in dichloromethane (2 mL). The color of the solution immediately changed from orange to purple. The solution was evaporated, and the resulting purple solid was washed with pentane. The solid was then dissolved in 3 mL fluorobenzene and was layered with cold pentane and kept at -40 °C to give the product $[(C_6F_5)_3B\text{-}ON{=}NO\text{-}B(C_6F_5)_3][Cp_2Fe]_2$ (**7**-$[Cp_2Fe]_2$) (0.130 g, 63% yield) as purple crystals.

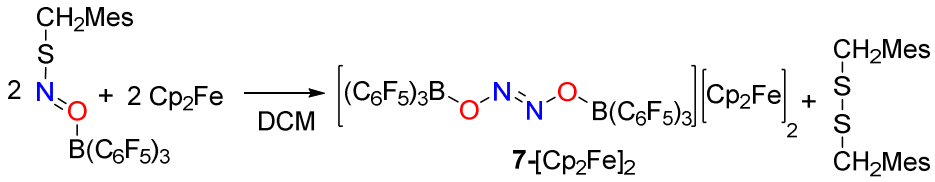

Scheme S9. Reduction of $MesCH_2SNO$-BCF (**4**) with Cp_2Fe.

14. EPR Analysis for the Reduction of ASNO-B(C_6F_5)$_3$ (3) with Cp^*_2Co

A fluorobenzene solution of decamethylcobaltocene (10 mM, 0.5 ml) in an EPR tube was slowly layered with a pentane solution of AdSNO-BCF (**3**) (23 mM, 0.217 ml) at RT. The EPR tube was capped and transferred outside the glovebox without shaking. The tube was then shaken couple of times and quickly placed in the EPR instrument.

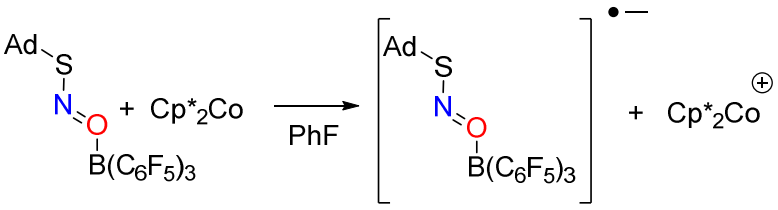

5

Scheme 10. Reduction of AdSNO-BCF (**3**) with Cp^*_2Co to generate [AdSNO-BCF]$^{\bullet/-}$ (**5**).

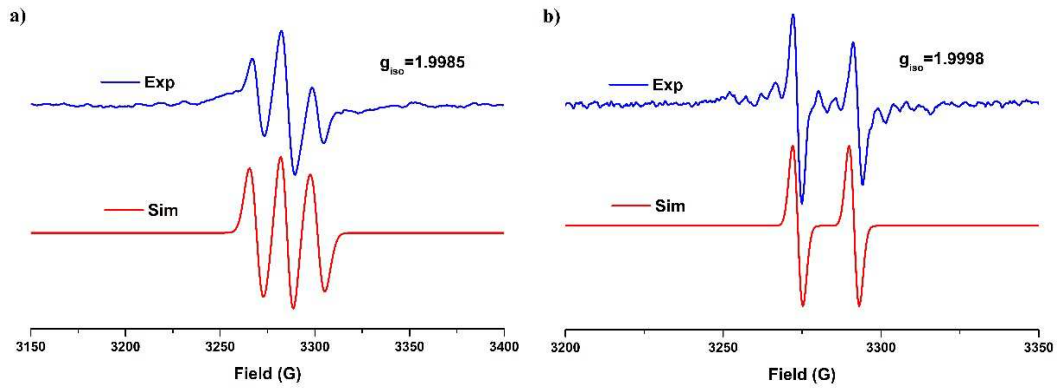

Figure S37. Isotropic X-band EPR spectra (blue trace) and simulation (red trace) of the reaction between (a) AdSNO-BCF (**3**) or (b) AdS^{15}NO-BCF (**3-^{15}N**) and Cp^*_2Co to generate radical anions **5-^{14}N** and **5-^{15}N**, respectively, in a mixture of fluorobenzene/pentane at 25 °C. Frequency =9.194384 GHz, power = 0.99 mW, ModWidth = 15 mT, time-constant = 0.03 s. Simulation provides g_{iso} = 1.9985, A_{iso}(^{14}N) = 45.0 MHz and W_{iso} = 2.7 mT (for **3**), and g_{iso} = 1.9998, A_{iso}(^{15}N) = 62.5 MHz, W_{iso} = 2.1 mT (for **3-^{15}N**). As expected, the ratio of isotropic ^{15}N and ^{14}N hyperfine coupling constants A(^{15}N)/A(^{14}N) = 1.38 is very close to the ratio of their gyromagnetic ratios γ(^{15}N)/γ(^{14}N) =1.40.

15. Crystallographic Details and Additional Structures

Single crystals of each compound AdSNO-B(C_6F_5)$_3$ (**3**) (CCDC 1945525), MesCH_2SNO-B(C_6F_5)$_3$ (**4**) (CCDC 1945527), [(C_6F_5)$_3$B-ON=NO-B(C_6F_5)$_3$][Cp^*_2Co]$_2$ (**7**-[Cp^*_2Co]$_2$) (CCDC 1945528), [(C_6F_5)$_3$B-ON=NO-B(C_6F_5)$_3$][Cp_2Fe]$_2$ (**7**-[Cp_2Fe]$_2$) (CCDC 1945529) were mounted under mineral oil on a Mitegen micromount and immediately placed in a cold nitrogen stream at 100(2) K prior to data collection. Data for compounds **3**, **7**-[Cp^*_2Co]$_2$, and **7**-[Cp_2Fe]$_2$ were collected on a Bruker D8 Quest equipped with a Photon100 CMOS detector and a Mo ImS source. Data for **4** were collected on a Bruker DUO equipped with an APEXII CCD detector and Mo fine-focus sealed source. A series of 0.5^o φ- and ω-scans were collected with monochromatic Mo Kα radiation, λ = 0.7107 Å and integrated with the Bruker SAINT program. Structure solution and refinement was performed using the SHELXTL/PC suite and ShelXle. Intensities were corrected for Lorentz and polarization effects and an empirical absorption correction was applied using Blessing's method as incorporated into the program SADABS. Non-hydrogen atoms were refined with anisotropic thermal parameters and hydrogen atoms were included in idealized positions unless otherwise noted. Further comments on structural models:

[AdSNO-BCF] (C_5H_{12})$_{0.5}$ (3). One half occupied lattice pentane solvent molecule is present in the lattice. This molecule is disordered across a symmetry site. The like C-C distances were restrained to be similar.

[(C_6F_5)$_3$B-ON=NO-B(C_6F_5)$_3$][Cp_2^*Co]$_2$ (7-[Cp^*_2Co]$_2$**).** A total of eight highly disordered fluoro-benzene solvent molecules per unit cell were removed from the model using the SQUEEZE routine in PLATON. Attempts to model the disordered solvent molecules resulted in non-convergence, thus they were removed.

[(C_6F_5)$_3$B-ON=NO-B(C_6F_5)$_3$][Cp_2Fe]$_2$ (7-[Cp_2Fe]$_2$**).** The data was refined as a two component twin. The ratio of the twin domains refined to ~69:31, and the twin law by rows was (-1 0 0), (0 -1 0), (.113 0 1). Two C6F5 groups are disordered over two orientations. The like C-F and C-C distances were restrained to be similar. The C1/C1B and C31/C31B atom pairs were constrained to have equal x,y,z positions and equal anisotropic displacement parameters.

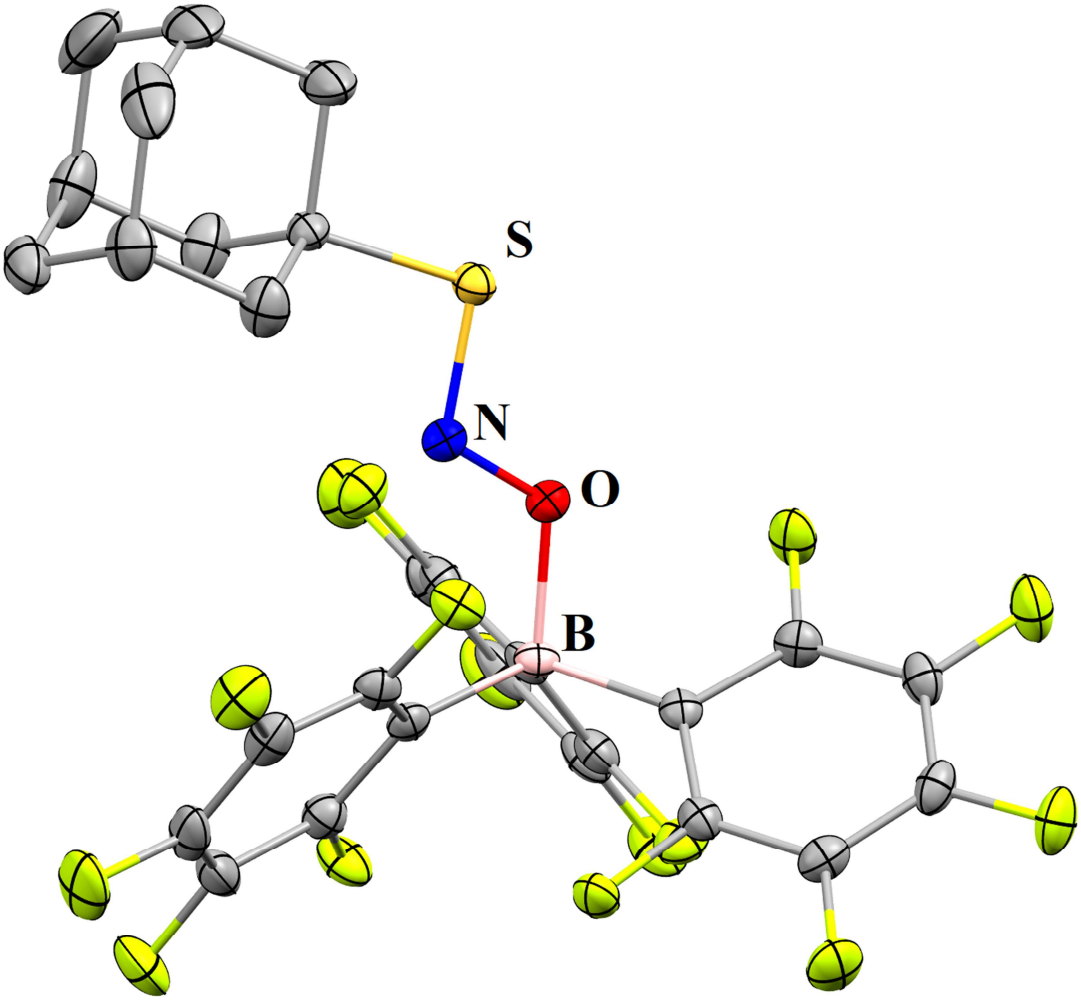

Figure S38. Molecular structure of AdSNO-BCF (**3**) (CCDC 1945525). The thermal ellipsoid plots are drawn at 50% probability level. Hydrogen atoms are omitted for clarity. Selected bond distances (Å) and angles (°): S-N 1.6252(17), N-O 1.278(2), O-B 1.612(3), S-N-O 112.37(13), N-O-B 118.74(14).

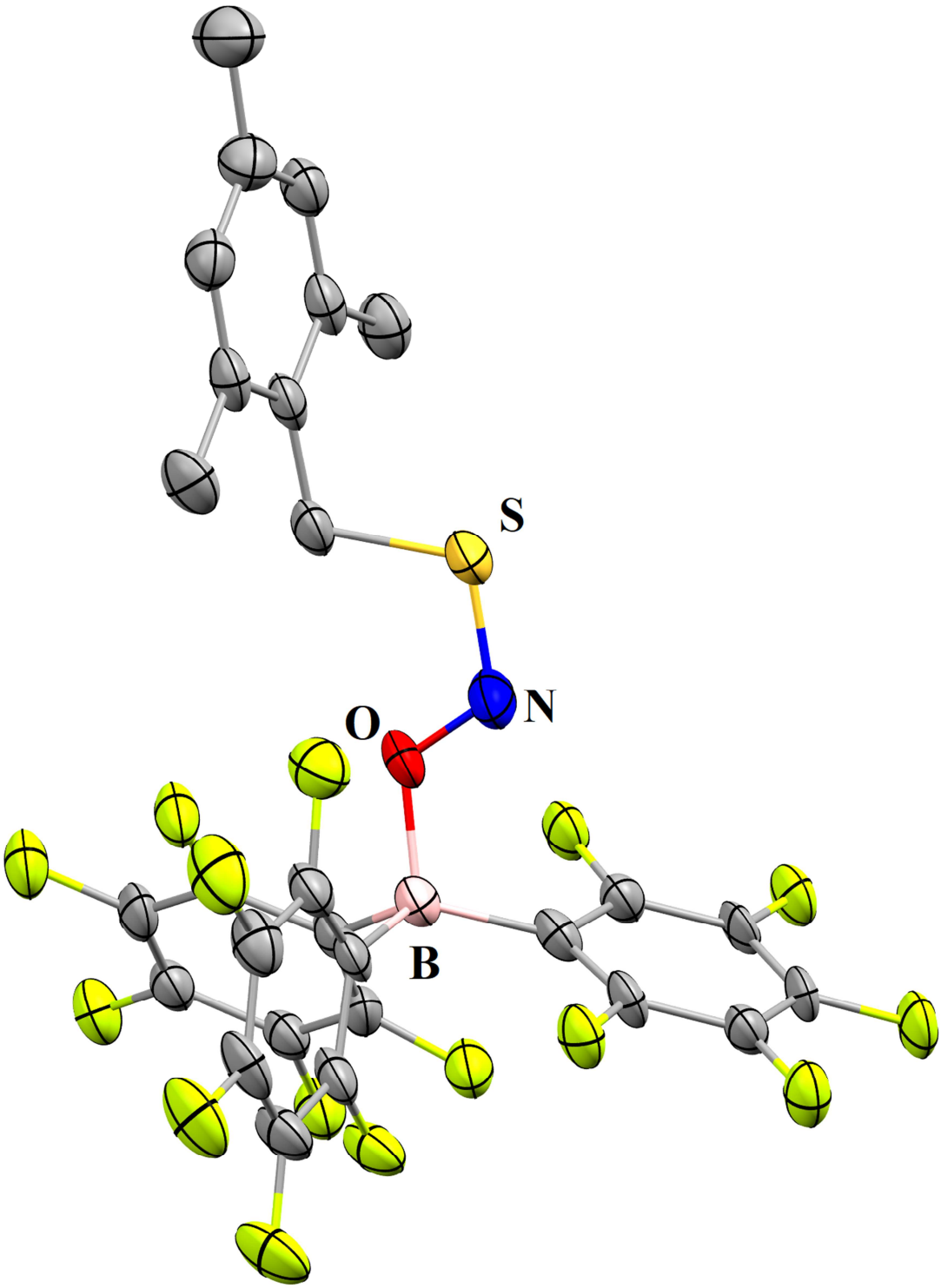

Figure S39. Molecular structure of $MesCH_2SNO$-BCF (**4**) (CCDC 1945527). The thermal ellipsoid plots are drawn at 50% probability level. Hydrogen atoms are omitted for clarity. Selected bond distances (Å) and angles (°): S-N 1.608(5), N-O 1.274(5), O-B 1.586(7), S-N-O 116.0(4), N-O-B 116.9(4).

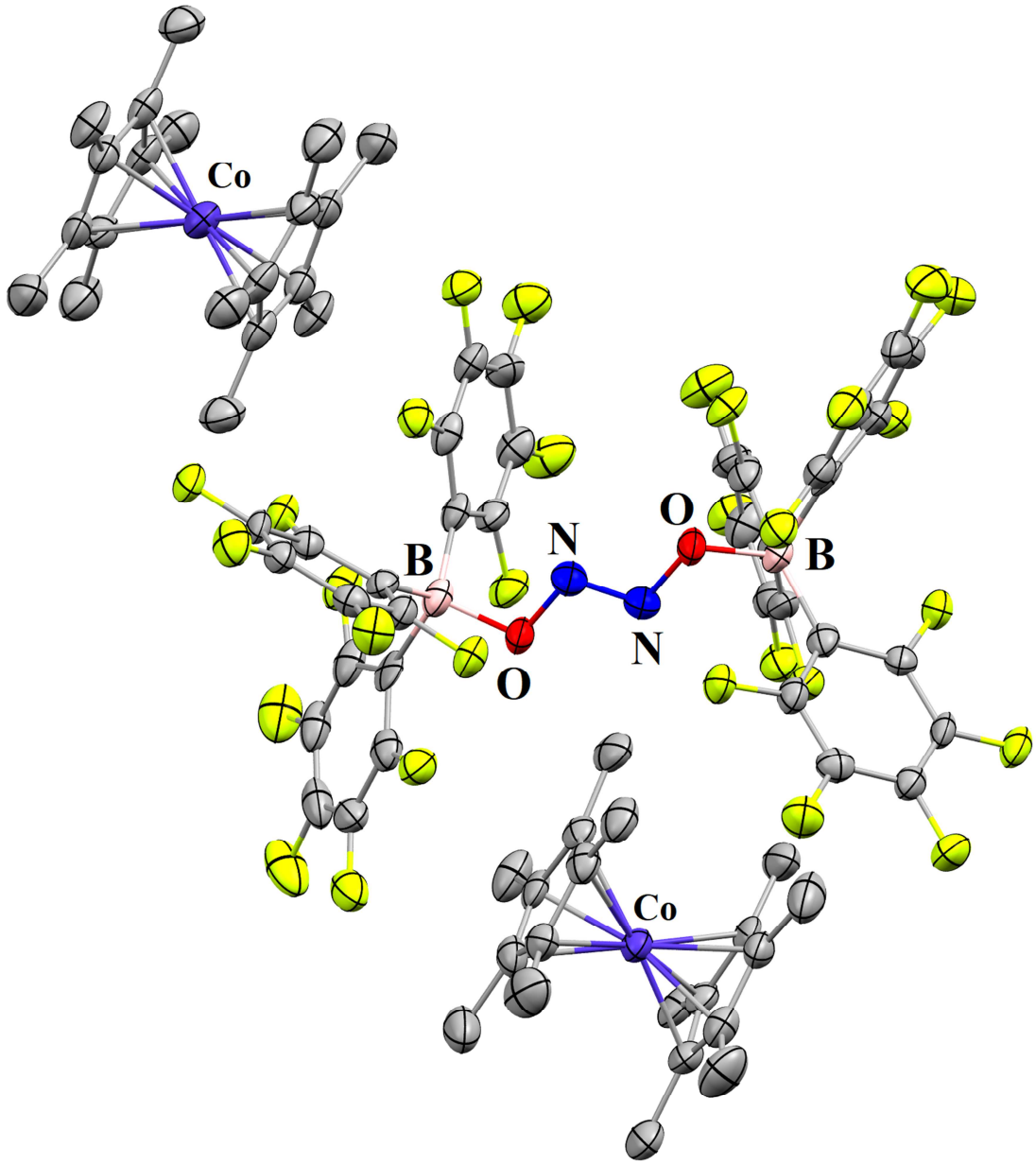

Figure S40. Molecular structure of $[(C_6F_5)_3B\text{-}ON{=}NO\text{-}B(C_6F_5)_3][Cp^*_2Co]_2$ (**7**-$[Cp^*_2Co]_2$) (CCDC 1945528). The thermal ellipsoid plots are drawn at 50% probability level. Hydrogen atoms are omitted for clarity. Selected bond distances (Å) and angles (°): N-O 1.381(6), N-N 1.257(9), O-B 1.489(7), O-N-N 106.5(5), N-O-B 109.0(4).

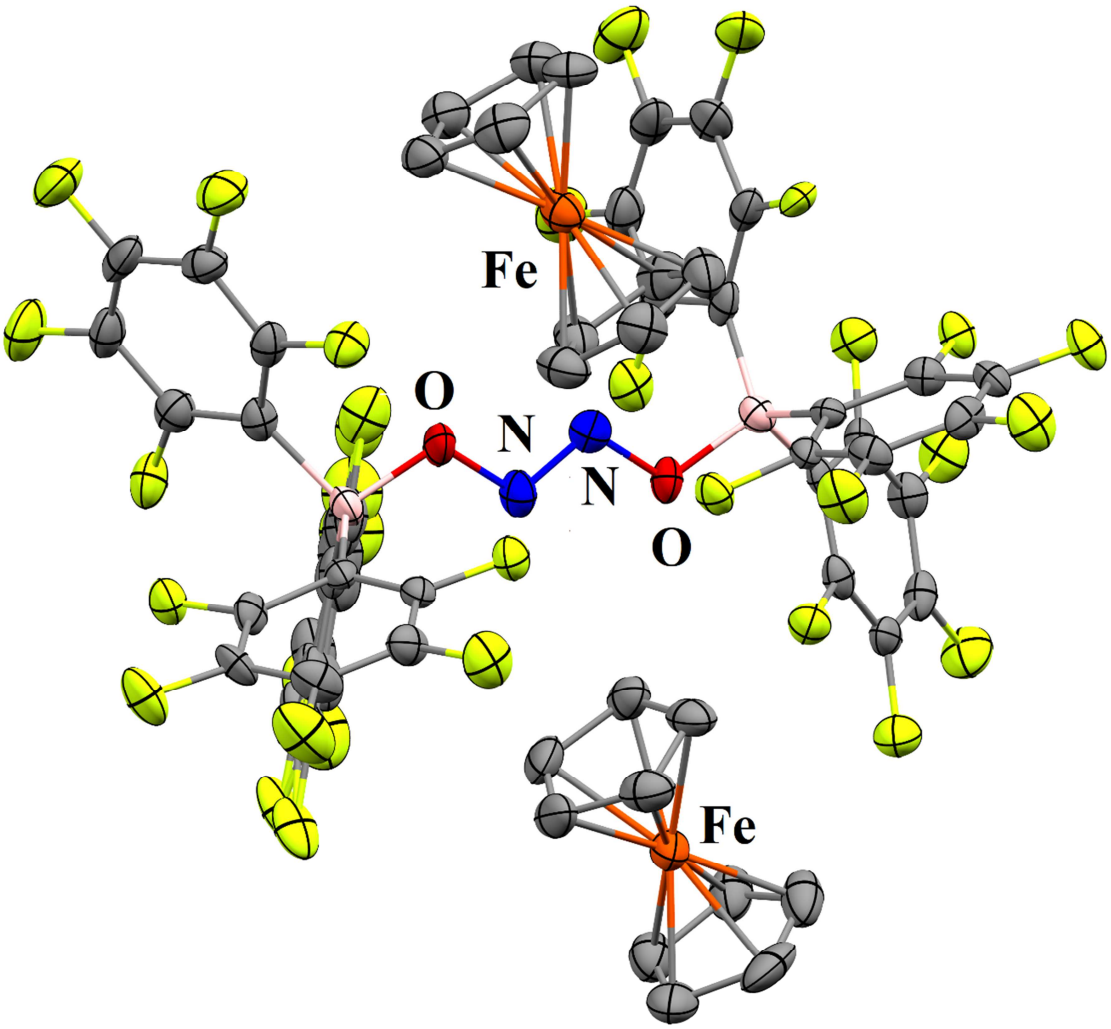

Figure S41. Molecular structure of $[(C_6F_5)_3B\text{-}ON{=}NO\text{-}B(C_6F_5)_3][CpFe]_2$ (**7**-$[Cp_2Fe]_2$) (CCDC 1945529). The thermal ellipsoid plots are drawn at 50% probability level. Hydrogen atoms are omitted for clarity. Selected bond distances (Å) and angles (°): N1-O1 1.380 (4), N2-O2 1.364 (4), N1-N2 1.274 (4), O1-B1 1.492(6), O2-B2 1.505(6), N1-O1-B1 113.8 (4), N2-O2-B2 111.9 (3), N2-N1-O1 107.0 (4), N1-N2-O2 106.3 (4).

16. Computational Details and Results

Electronic structure calculations were performed using density functional theory (DFT) with ωB97XD range-separated density functional with empirical dispersion correction;[4] previous benchmarking of the performance of the DFT methods for the RSNO compounds against high-level ab inito results[5] demonstrated a good performance of the ωB97XD functional for description of the –SNO group properties. A triple-zeta quality basis set augmented with diffuse functions, ma-def2-TZVPP, has been used throughout; preliminary calculations also employed smaller ma-def2-SV(P) basis set.[6] Due to the system size, calculations of structures including more than one $B(C_6F_5)_3$ moieties (Figures S46-S48) used a reduced ma-def2-SV(P) basis set, red-ma-def2-SV(P), with removed diffuse and polarization basis functions on F atoms and removed diffuse functions on C atoms.

Solvent (dichloromethane) effects have been treated using the integral equation formalism polarizable continuum model (IEFPCM) as implemented in Gaussian 16.[7]

Harmonic frequency calculations have been performed for all optimized structures to ascertain the nature of the stationary point found; thermodynamic parameters have been calculated within harmonic approximation for the T=298 K, 1 M standard state.

NMR chemical shifts were calculated with the standard Gauge-Independent Atomic Orbital (GIAO) method.[8] Atomic spin populations were evaluated with Natural Population Analysis (NPA).[9]

The relative contributions of the resonance structures ***S***, ***D***, and ***I*** (Figure 1A in the main text) have been estimated using Natural Resonance Theory (NRT) approach as implemented in the NBO 7.0 code.[10] The NRT calculations used a local NRT variant, where only the resonance structures arising from the –SNO group have been considered. To ensure consistency of the NRT results across the different molecules/complexes, the three resonance structures ***S***, ***D***, and ***I*** have been used as the reference structures for the NRT calculation and the NRTPAR parameter has been set to 99%.

Cartesian coordinates for calculated structures may be found in an accompanying supporting information file.

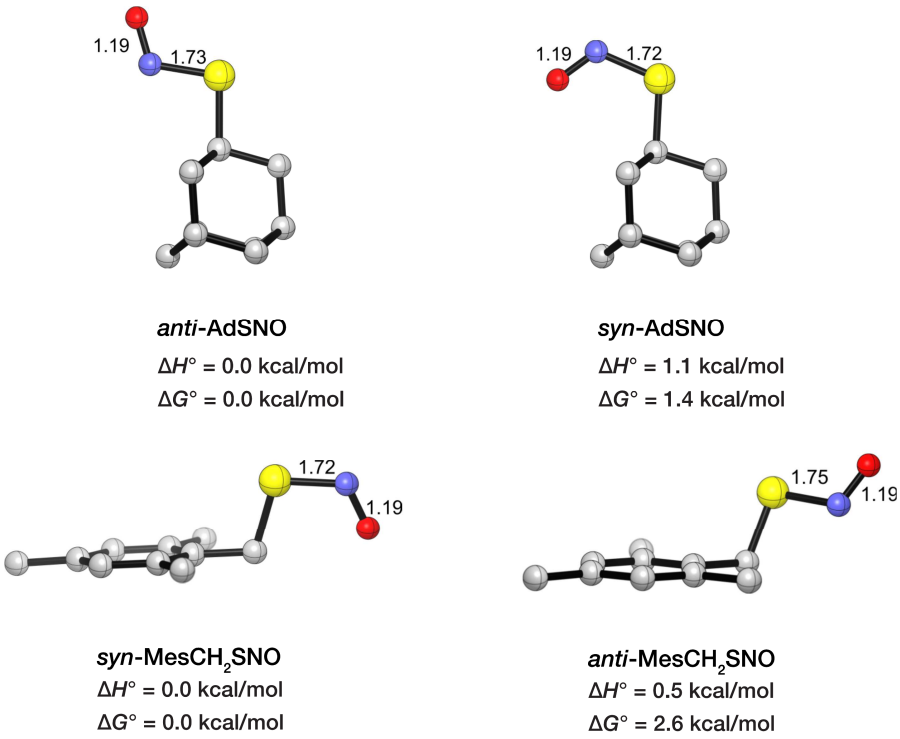

Figure S42. Structures and relative free energies of AdSNO and $MesCH_2SNO$ conformers calculated at the ωB97XD-PCM(CH_2Cl_2)/ma-def2-TZVPP level. Bond lengths in Å; hydrogen atoms not shown for clarity.

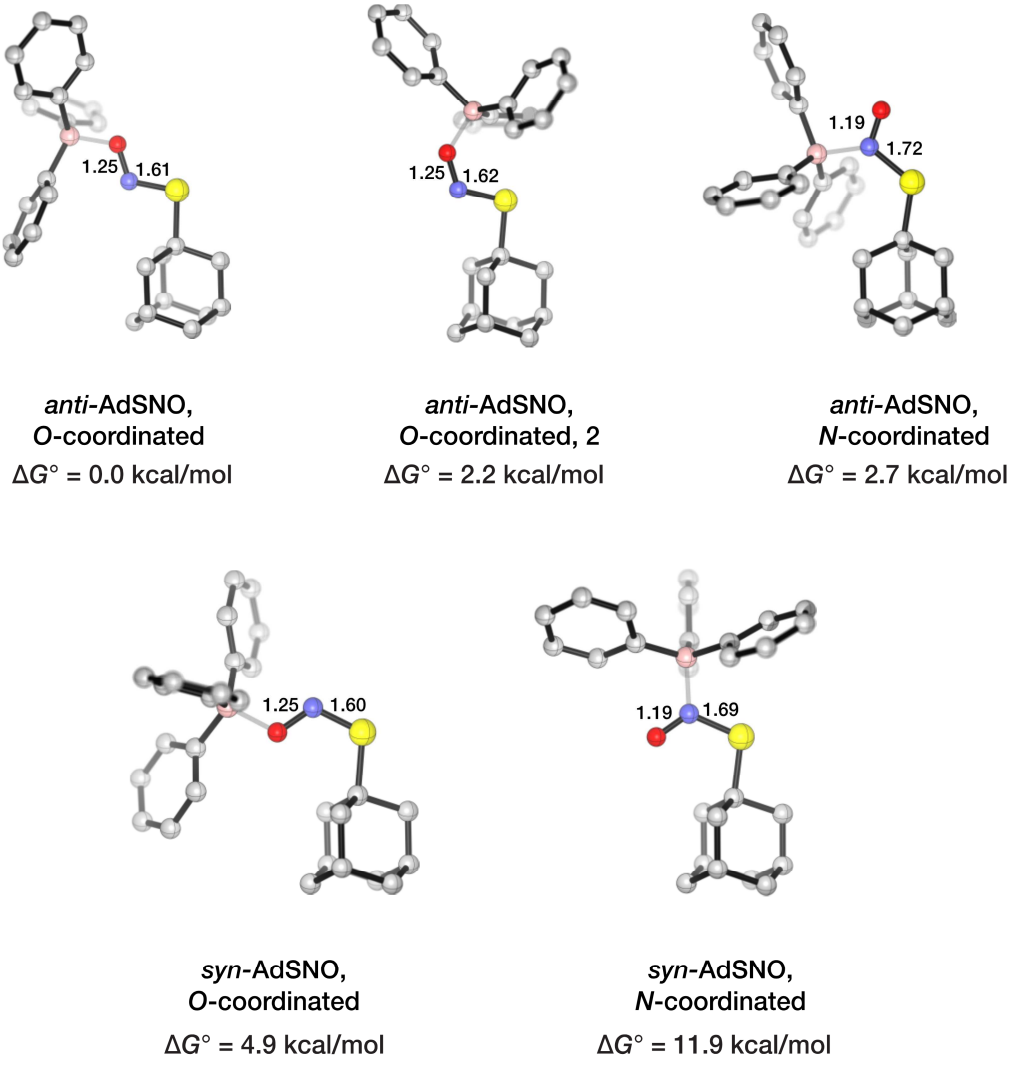

Figure S43. Structures and relative free energies of AdSNO-B(C_6F_5)$_3$ complexes calculated at the ωB97XD-PCM(CH_2Cl_2)/ma-def2-TZVPP level. Bond lengths in Å; hydrogen and fluorine atoms not shown for clarity.

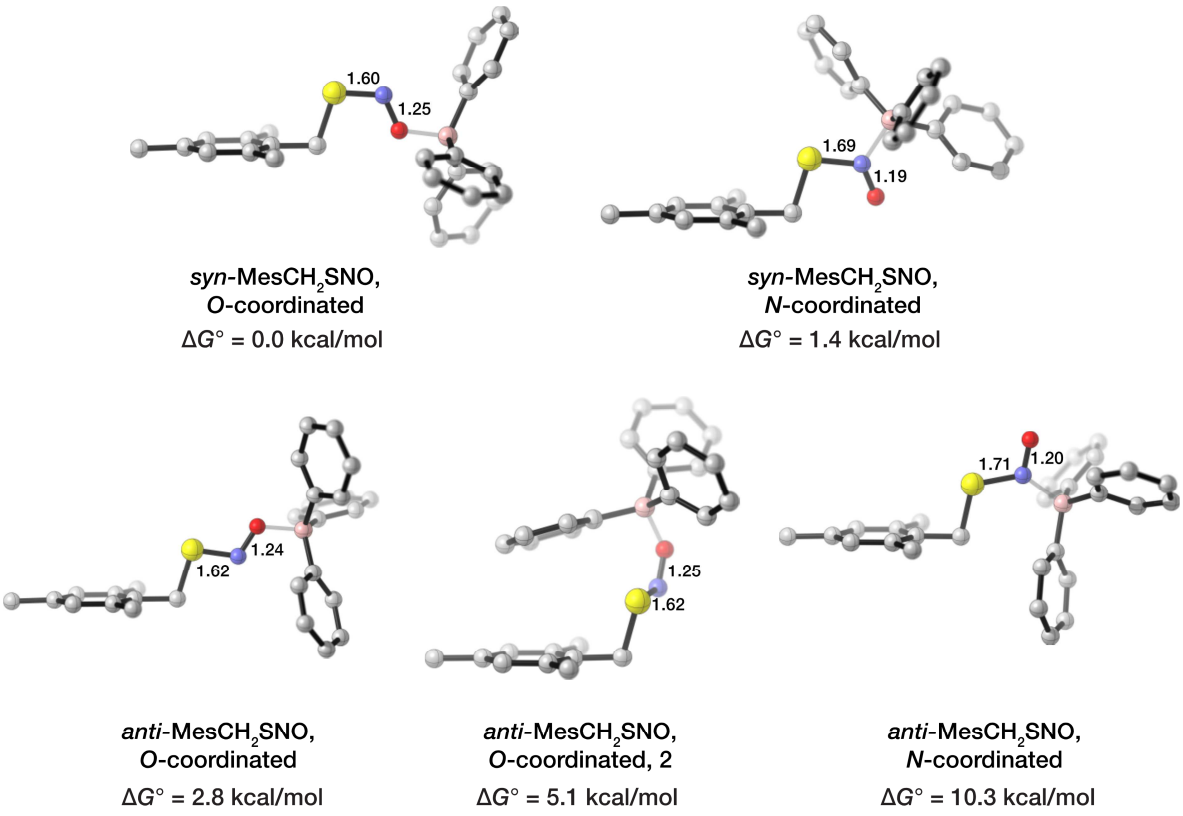

Figure S44. Structures and relative free energies of $MesCH_2SNO\text{-}B(C_6F_5)_3$ complexes calculated at the ωB97XD-PCM(CH_2Cl_2)/ma-def2-TZVPP level. Bond lengths in Å; hydrogen and fluorine atoms not shown for clarity.

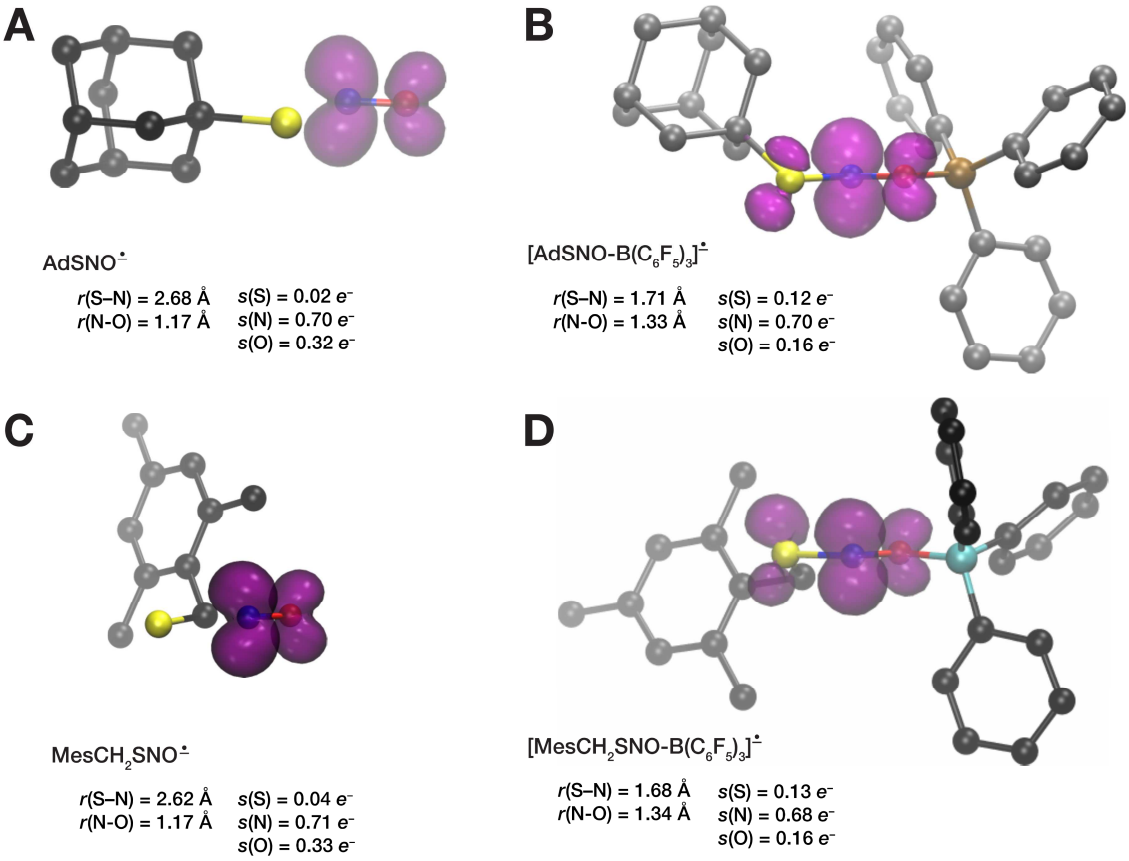

Figure S45. Unpaired spin density distribution (0.004 au isosurfaces) in RSNO anion-radicals (**A**, **C**) and the corresponding RSNO-B(C_6F_5)$_3$ anion-radicals (**B**, **D**) with corresponding S–N and N–O bond lengths and total spin populations ***s*** on the –SNO group atoms calculated at the ωB97XD-PCM(CH_2Cl_2)/ma-def2-TZVPP level. Hydrogen and fluorine atoms not shown for clarity.

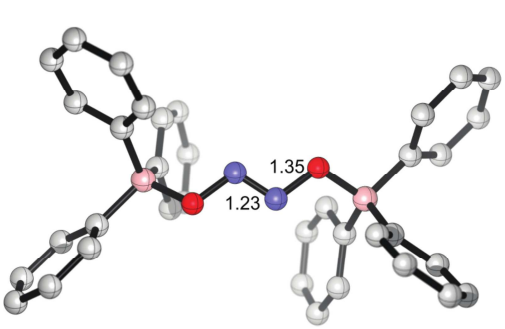

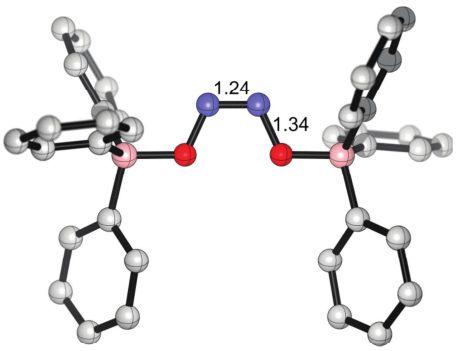

trans-$(C_6F_5)_3BO–N=N–OB(C_6F_5)_3^{2-}$

$\Delta G°$ = 0.0 kcal/mol
$\Delta H°$ = 0.0 kcal/mol

δ ^{15}N 425 ppm

cis-$(C_6F_5)_3BO–N=N–OB(C_6F_5)_3^{2-}$

$\Delta G°$ = +1.6 kcal/mol
$\Delta H°$ = +0.6 kcal/mol

δ ^{15}N 380 ppm

Figure S46. Two forms of $[(C_6F_5)_3BONNOB(C_6F_5)_3]^{2-}$ calculated at the ωB97XD-PCM(CH_2Cl_2)/red-ma-def2-SV(P) level: relevant bond lengths (Å), relative energies, and predicted ^{15}N NMR shifts. Hydrogen and fluorine atoms not shown for clarity.

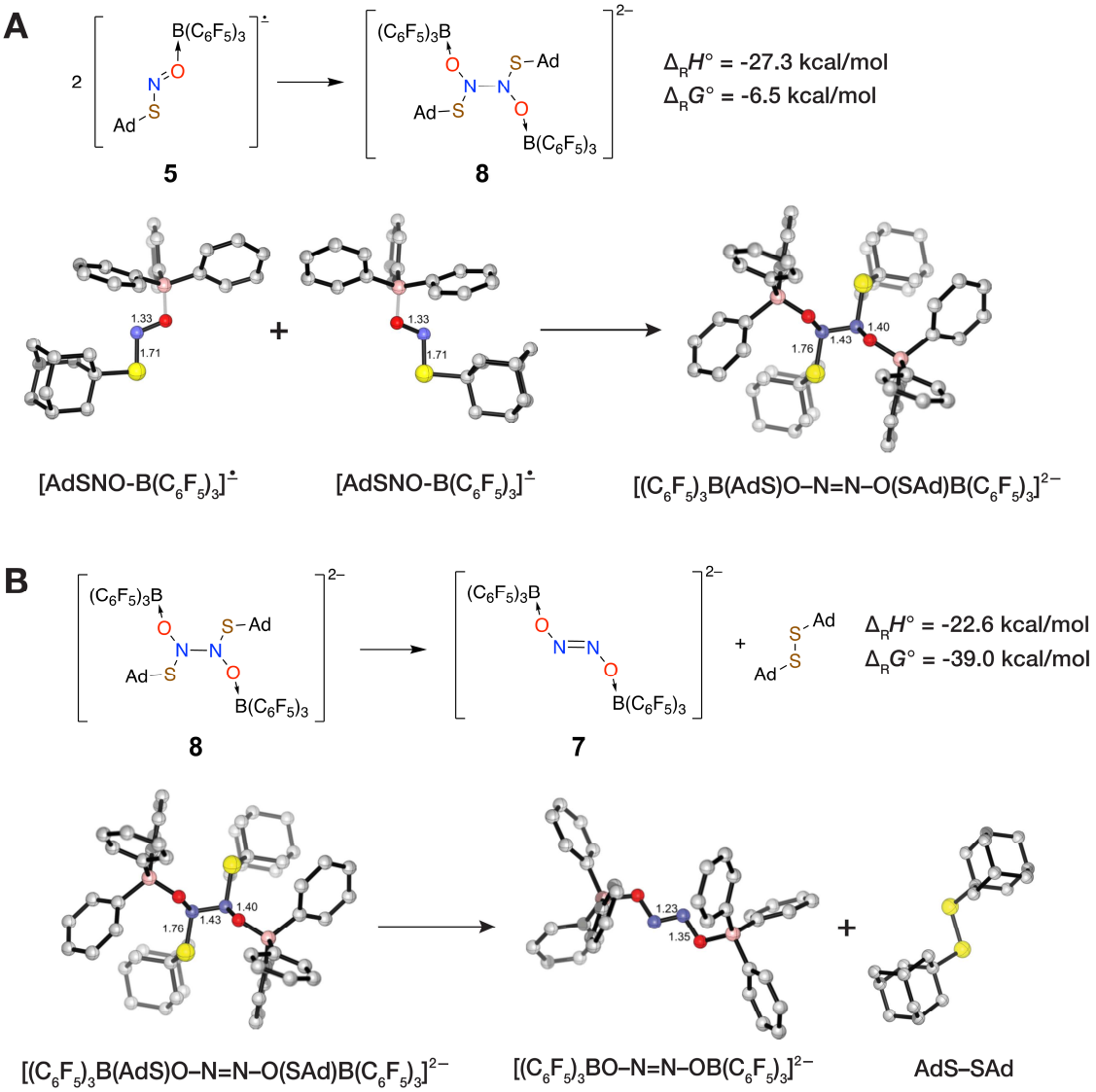

Figure S47. Thermodynamic parameters of (**A**) the dimerization reaction of the AdSNO-$B(C_6F_5)_3$ anion-radical and (**B**) subsequent AdS–SAd elimination calculated at the ωB97XD-PCM(CH_2Cl_2)/red-ma-def2-SV(P) level. Hydrogen and fluorine atoms not shown for clarity.

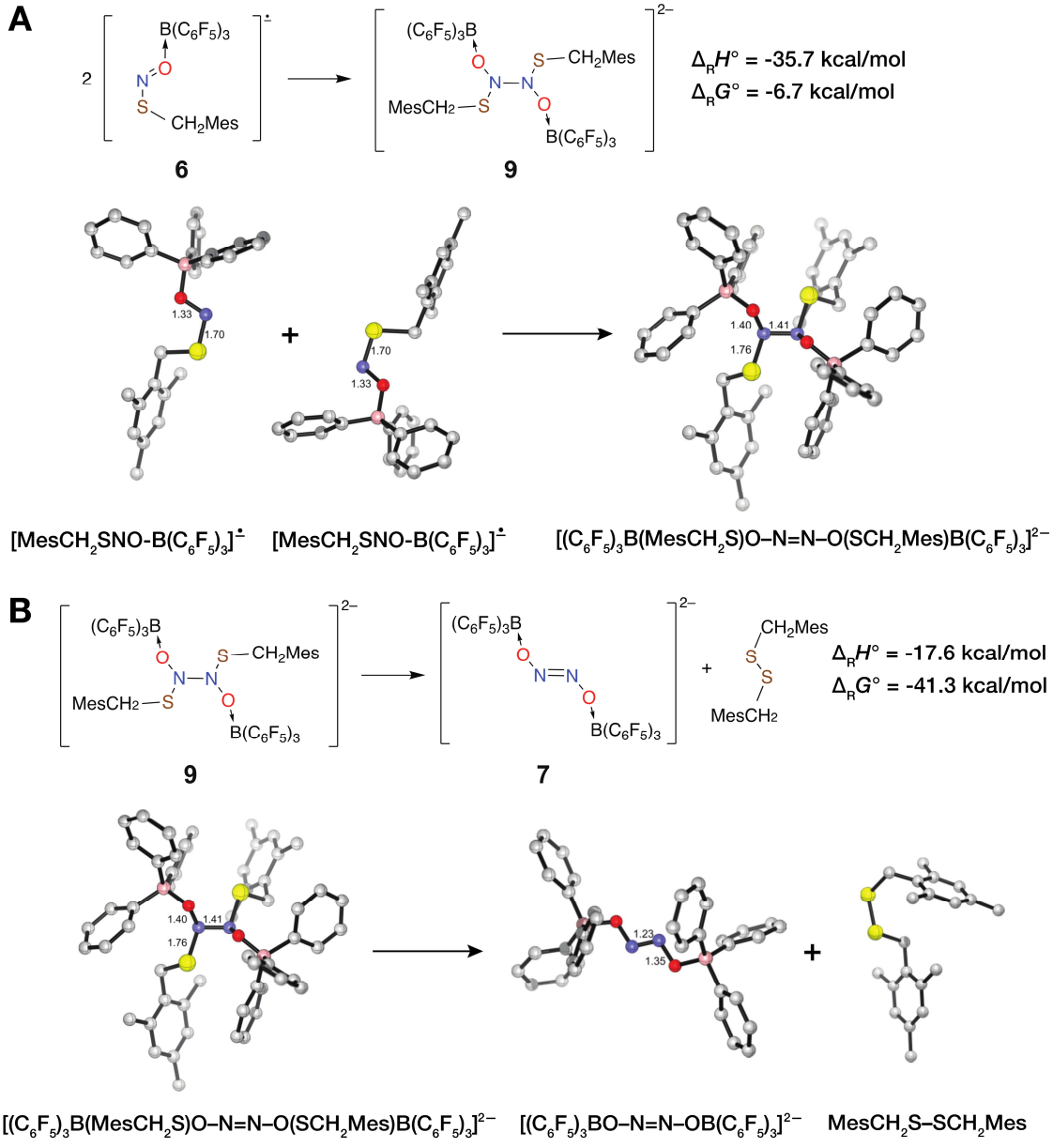

Figure S48 Thermodynamic parameters of (**A**) the dimerization reaction of the $MesCH_2SNO\text{-}B(C_6F_5)_3$ anion-radical and (**B**) subsequent $MesCH_2S–SCH_2Mes$ elimination calculated at the ωB97XD-PCM(CH_2Cl_2)/red-ma-def2-SV(P) level. Hydrogen and fluorine atoms not shown for clarity.

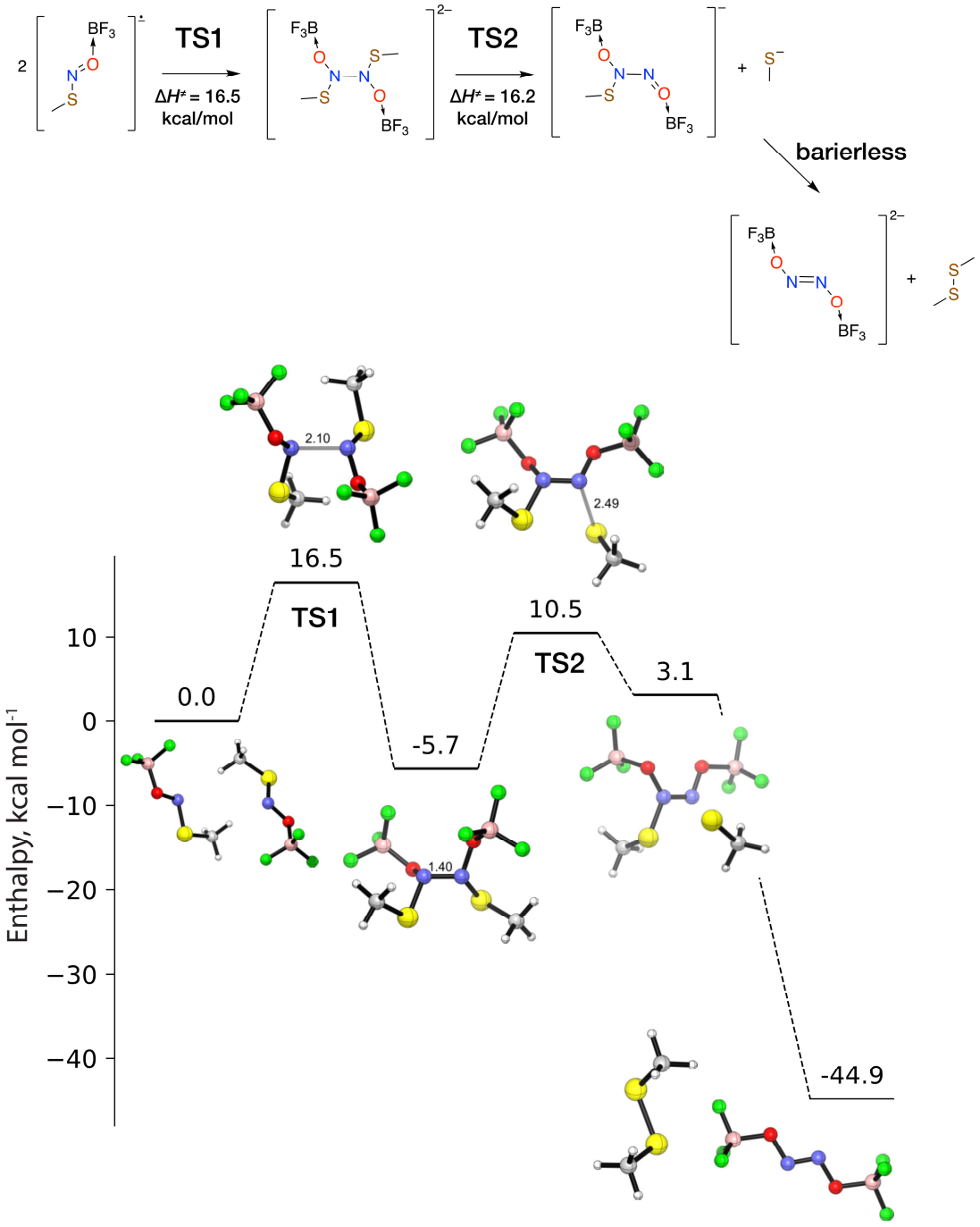

Figure S49. Full reaction profile for the dimerization reaction of the small model system, CH_3SNO-BF_3 anion-radical, and subsequent CH_3S–SCH_3 elimination calculated at the ωB97XD-PCM(CH_2Cl_2)/ma-def2-TZVPP level; broken-symmetry unrestricted calculations have been used for the open-shell TS1 structure ($\langle S^2 \rangle$=0.40); transition structures have been verified with IRC calculations. Bond lengths in Å.

17. References

[1] Girard, P.; Guillot, N.; Motherwell, W. B.; Hay-Motherwell, R. S.; Potier, P. *Tetrahedron*, **1999**, *55*, 3573-3584.

[2] Melzer, M. M.; Mossin, S.; Cardenas, A. J.; Williams, K. D.; Zhang, S.; Meyer, K.; Warren, T. H. *Inorg. Chem.* **2012**, *51*, 8658–8660.

[3] Kundu, S.; Kim, W. Y.; Bertke, J. A.; Warren, T. H. *J. Am. Chem. Soc.* **2017**, *139*, 1045-1048.

[4] J.-D. Chai, M. Head-Gordon *Phys. Chem. Chem. Phys.* **2008**, *10*, 6615-6620.

[5] D. G. Khomyakov, Q. K. Timerghazin, *J. Chem. Phys.* **2017**, *147*, 044305.

[6] a) F. Weigend, R. Ahlrichs *Phys. Chem. Chem. Phys.* **2005**, *7*, 3297-3305; b) J. Zheng, X. Xu, D. G. Truhlar, *Theor. Chem. Acc.* **2011**, *128*, 295-305.

[7] M. J. Frisch, G. W. Trucks, H. B. Schlegel, G. E. Scuseria, M. A. Robb, J. R. Cheeseman, G. Scalmani, V. Barone, G. A. Petersson, H. Nakatsuji, X. Li, M. Caricato, A. V. Marenich, J. Bloino, B. G. Janesko, R. Gomperts, B. Mennucci, H. P. Hratchian, J. V. Ortiz, A. F. Izmaylov, J. L. Sonnenberg, Williams, F. Ding, F. Lipparini, F. Egidi, J. Goings, B. Peng, A. Petrone, T. Henderson, D. Ranasinghe, V. G. Zakrzewski, J. Gao, N. Rega, G. Zheng, W. Liang, M. Hada, M. Ehara, K. Toyota, R. Fukuda, J. Hasegawa, M. Ishida, T. Nakajima, Y. Honda, O. Kitao, H. Nakai, T. Vreven, K. Throssell, J. A. Montgomery Jr., J. E. Peralta, F. Ogliaro, M. J. Bearpark, J. J. Heyd, E. N. Brothers, K. N. Kudin, V. N. Staroverov, T. A. Keith, R. Kobayashi, J. Normand, K. Raghavachari, A. P. Rendell, J. C. Burant, S. S. Iyengar, J. Tomasi, M. Cossi, J. M. Millam, M. Klene, C. Adamo, R. Cammi, J. W. Ochterski, R. L. Martin, K. Morokuma, O. Farkas, J. B. Foresman, D. J. Fox, Wallingford, CT, **2016**.

[8] J. R. Cheeseman, G. W. Trucks, T. A. Keith, M. J. Frisch *J. Chem. Phys.* **1998**, *104*, 5497-5509.

[9] A. E. Reed, R. B. Weinstock, F. Weinhold *J. Chem. Phys.* **1985**, *83*, 735-746.

[10] a) E. D. Glendening, J. K. Badenhoop, F. Weinhold *J. Comp. Chem.* **1998**, *19*, 628-646; b) E. D. Glendening, C. R. Landis, F. Weinhold, *J. Am. Chem. Soc.* **2019**, *141*, 4156-4166; c) E. D. Glendening, C. R. Landis, F. Weinhold *J. Comp. Chem.* **2019**, *40*, 2234-2241; d) E. D. Glendening, F. Weinhold *J. Comp. Chem.* **1998**, *19*, 610-627; e) E. D. Glendening, F. Weinhold *J. Comp. Chem.* **1998**, *19*, 593-609.